Vítor Manuel
Sousa Coelho

Antenas lente de feixe amplo impressas em 3D

3D-Printed wide beamwidth lens antennas

Vítor Manuel
Sousa Coelho

Antenas lente de feixe amplo impressas em 3D

3D-Printed wide beamwidth lens antennas

" *Every accomplishment starts with the decision to try.*"

— John F. Kennedy

Universidade de Aveiro
2021

Vítor Manuel Sousa Coelho

Antenas lente de feixe amplo impressas em 3D

3D-Printed wide beamwidth lens antennas

Dissertação apresentada à Universidade de Aveiro para cumprimento dos requisitos necessários à obtenção do grau de Mestre em Engenharia Eletrónica e Telecomunicações, realizada sob a orientação científica do Doutor (João Nuno Pimentel da Silva Matos), Professor associado do da Universidade de Aveiro, e do Doutor Tiago Miguel Valente Varum), Professor investigador do Instituto de Telecomunicações da Universidade de Aveiro.

o júri / the jury

presidente / president

Professor Doutor Armando Carlos Domingues da Rocha
Professor Auxiliar, Universidade de Aveiro

vogais / examiners committee

Professor Doutor Henrique Manuel de Castro Faria Salgado
Professor Associado, Universidade do Porto

Professor Doutor João Nuno Pimentel da Silva Matos
Professor Associado, Universidade de Aveiro (orientador)

agradecimentos / acknowledgements

Gostaria de começar por agradecer aos meus pais, Ricardo e Marla Coelho, que, apesar de estar há mais cinco anos a estudar longe de casa e passar a maioria do ano sem os ver, ainda se preocupam e ajudam tanto como no primeiro dia que saí de casa e atravessei meio oceano Atlântico para começar o meu percurso académico.

Também quero agradecer à Carolina Soares que durante estes anos todos me acompanhou nesta nossa aventura longe de casa e teve a paciência e amor para me apoiar todos estes anos. Não me posso esquecer, como é óbvio, todos os colegas, amigos e companheiros que durante todos estes anos me ajudaram a tornar a cidade de Aveiro a minha segunda casa.

Quero agradecer ainda ao orientador Professor João Nuno Matos e ao meu co-orientador Professor Tiago Varum, por toda a disponibilidade (para esclarecimento de dúvidas e discussão de problemas) e todos os conhecimentos transmitidos.

Deixo o meu agradecimento ao Hugo Mostardinha e ao Paulo Gonçalves, pelos auxílios prestados na fabricação e testagem dos protótipos desenvolvidos.

Por último gostaria de agradecer ao Instituto de Telecomunicações de Aveiro, ao Departamento de Electrónica, Telecomunicações e Informática e à Universidade de Aveiro por me ter disponibilizado todas as condições, ferramentas e conhecimentos que culminaram na realização deste trabalho.

Palavras Chave

antenas lente, impressão 3D, antena patch, largura de feixe, materiais dielétricos.

Resumo

A recente evolução das radiocomunicações combinada com as inovadoras técnicas de fabrico, como a impressão 3D, impulsionaram o desenvolvimento e implementação de antenas com novas estruturas fabricadas com materiais incomuns. Um exemplo deste tipo de evolução são as antenas lente.

As antenas lente estão sempre associadas a uma antena fonte (usualmente uma antena microstrip patch) e permitem alterar as caraterísticas de radiação (variar o ganho ou a directividade) da antena fonte. Assim, as lentes podem ser usadas para melhorar o desempenho de alguns tipos de sistema radiantes, como por exemplo o caso dos phased arrays, utilizados para fazer beamforming. No entanto, estes apresentam algumas limitações de cobertura, devido aos seus elementos do array terem ganho diretivo variável na zona de interesse. A utilização duma antena lente faz com que ocorra a alteração do diagrama de radiação de modo a obter uma maior largura de feixe podendo ser uma solução para referida limitação.

Ao longo desta dissertação foi estudada a possibilidade de se utilizarem lentes para aumentar a largura de feixe de uma simples antena microstrip patch. Para isso, foram estudadas e realizadas simulações de várias estruturas de antenas lente com uma antena patch (calibrada para os 7.8GHz) com o intuito de determinar qual o comportamento do conjunto e verificar a possibilidade de tornar mais uniforme o diagrama de radiação no semi-espaço pretendido .

A produção de protótipos de antenas lente com a impressão 3D requer o conhecimento das características elétricas dos materiais de fabrico (PLA, PETG e nylon), mais precisamente sua constate dielétrica. Para tal, foi feita uma caracterização de várias amostras desses materiais tendo em conta diferentes condições de fabrico.

A última etapa foi a fabricação, por impressão 3D, de protótipos de antenas e lentes, utilizando diferentes materiais e condições de fabrico. No total foram fabricadas nove lentes (seis com uma estrutura de um único material e três com vários materiais distintos) e sete antenas patch (cinco de polarização linear e duas de polarização circular).

Finalmente foi feito um estudo comparativo dos resultados obtidos por simulação com as medidas realizadas em câmara anecoica tanto para as antenas patch, como para o conjunto antena lente.

Keywords lens antennas, 3D printing, patch antenna, beamwidth, dielectric materials.

Abstract

The recent evolution of radio communications combined with innovative manufacturing techniques, such as 3D printing, has driven antennas development and implementation of new structures made of unusual materials. An example of this type of evolution are the lens antennas.

Lens antennas are always associated with a source antenna (usually a microstrip patch antenna) and allow changing the source antenna's radiation characteristics (varying the gain or directivity). Thus, lenses can improve the performance of some types of communication systems, such as phased arrays, which are used for beamforming. However, they have some limitations in coverage due to the array elements having low directivity. The use of a lens antenna changes the radiation diagram to obtain a wider beamwidth and is a potential solution to the problem of phased arrays.

Throughout this dissertation, was studied the possibility of using lens antennas to change the radiation beam and increase the beamwidth of a simple microstrip patch antenna. For this purpose, simulations of several lens antenna structures were performed with a patch antenna (calibrated for 7.8GHz) to determine the array's behavior and verify if it is possible to increase the beamwidth.

One of the requirements to produce prototypes of lens antennas with 3D printing is knowing the electrical characteristics of the manufacturing materials (PLA, PETG, and nylon), more precisely, their dielectric constant. For that several samples of these materials were characterized considering different manufacturing conditions.

The last step is the fabrication, by 3D printing, of prototype antennas using different materials and fabrication conditions. Nine lenses (six with a single material structure and three with several different materials) and seven patch antennas (five linearly polarized and two circularly polarized) were fabricated.

Finally, was made a comparative study of the results obtained by simulation with the measurements performed in an anechoic chamber for both the patch antennas and the lens antenna array.

Contents

List of Figures

List of Tables

List of Acronyms

5G	Fifth Generation of mobile communications
3D	Three Dimensional
LP	Linear Polarization
MHMFE	Modified Half Maxwell Fish-Eye
RF	Radiofrequency
RADAR	Radio Detection And Ranging
HPBW	Half-Power Beamwidth
HMFE	Half Maxwell Fish-Eye
MFE	Maxwell Fish-Eye
SEI	Simple Elliptical Integrated
FDM	Fused Deposition Modeling
SMLC	Single Microstrip Line Characterization
VNA	Vector Network Analyzer
CNC	Computer Numerical Control
CP	Circular Polarization
RHCP	Right Hand Circular Polarization
LHCP	Left Hand Circular Polarization
CE3	Creality Ender 3
UM3E	Ultimaker 3 Extended
IT	Instituto de Telecomunicações
PETG	Polyethylene Terephthalate Glycol
PLA	Polylactic Acid
SMA	SubMiniature version A
DETI	Departamento de Eletrónica, Telecomunicações e Informática

CHAPTER 1

Introduction

This chapter will provide a brief introduction for this dissertation, explaining the motivation and its contextualization.

1.1 Motivation and Contextualization

Radio communications are among the most important technologies of modern life, and present in mobile phones, cars, television, satellite, and many more. These applications can be in the frequency range from tens of kHz to hundreds of GHz.

Antennas are fundamental parts of a radio system. These antennas may have different shapes and construction methods, depending on the technology and frequency they operate. The current trend in Radiofrequency (RF) applications (such as Fifth Generation of mobile communications (5G) or Radio Detection And Ranging (RADAR)) is to use higher frequencies due to:

- In most national and international regulations and standards, the electromagnetic spectrum is already reserved for specific applications. Adding new applications between reserved frequencies is a very complicated and expensive process. Therefore, it is preferable to use higher frequency ranges because there are more frequencies available, and it also allows the use of more bandwidth.
- Superior data rates will require greater bandwidths, so having a higher carrier frequency allows more bandwidths and consequently a wider communication channel.
- The miniaturization of communication systems (such as smartphones) leading to less available space for antennas. Therefore, using higher frequencies (lower wavelengths) will lead to smaller antennas.

These factors create the need for new improved antenna structures that comply with the demands of those systems because sometimes the traditional antenna (such as patch, horn, and dipole antennas) do not have the expected performance for these systems.

Phased arrays are one of the most popular solutions. Those arrays consist of several radiating elements that are arranged and fed in a way that allows the control of its radiation

pattern. However, this control is limited because the angular coverage of the phased arrays is highly dependent on the radiation pattern of its elements that are not omnidirectional or isotropic elements (do not radiate equally in all directions). Usually, this type of array uses as elements microstrip antennas that are directive antennas with beamwidth around 70°.

There are different structures capable of altering the radiation pattern of an antenna, such as lens antennas. Those lenses (commonly manufactured dielectric materials) work together with a source antenna, usually a patch or a horn element, and allow to modify of the source antenna's radiation properties, for instance, the gain or directivity with or beamwidth [1]. An example of a lens antenna that provides a broader beamwidth from a simple patch antenna is the Modified Half Maxwell Fish-Eye (MHMFE) lens structure proposed in [2].

The use of new unconventional materials (such as dielectric polymers) and new manufacturing techniques have promoted the development of new antenna structures. An example of these new manufacturing techniques in dielectric materials is based on Three Dimensional (3D) printers, which have become increasingly common in all applications. They allow the modulation and manufacture of a prototype in a matter of hours at a low cost with a varied choice of production materials. This manufacturing technique also allows the fabrication of a new assortment of antennas, which were previously difficult or expensive to build [3].

The use of 3D printed lens antennas, such as the MHMFE, is a possible solution for the phased arrays coverage limitations, as combining a simple microstrip element of the array with the correct lens antenna will result in a wide beamwidth element, thus phased arrays with better coverage.

1.2 Objectives and methodology of the dissertation

This dissertation explores the use of lens antennas to change the radiation pattern and other parameters of the source antennas. More specifically, it is intended to explore the viability of using a lens that significantly increases the beamwidth of a traditional patch antenna. In particular, the MHMFE structure that can manipulate the radiation beam and increase its Half-Power Beamwidth (HPBW) to more than 160° [2]. This research is a step to understand if the phased arrays coverage limitations can be solved by adding lens antennas to array elements. However, this dissertation will only address this concept applied to a single patch antenna.

The main objective is to design a lens antenna that increases the beamwidth of a patch antenna and evaluate the possibility of manufacturing using 3D printing. To accomplish this objective, it will be required to perform an analysis of the lens antennas state of the art to understand how they work, their characteristics, and the most suitable manufacturing methods. Simulate the antenna's structure to ensure that the antenna works as intended and optimizes its operation. Characterize the dielectric materials used in the lens structure. The last stage is to manufacture and test the prototypes to ensure that it works as in the simulations.

1.3 Dissertation structure

This dissertation is divided into six chapters, each of them addressing a relevant topic of the dissertation, as described below:

- **Chapter 1** – The opening chapter of this dissertation intends to introduce the motivations and objectives.
- **Chapter 2** – The second chapter is a research about lens antennas to understand how they work and which types of lens antennas are best suited to the proposed objectives. Also, this chapter helps to understand which manufacturing techniques and construction materials are plausible to fabricate lens antennas.
- **Chapter 3** – This chapter analyzes lens antenna structures using simulations to understand if they work as indicated in state-of-the-art and if it is possible to fabricate using 3D printing.
- **Chapter 4** – The fourth chapter presents the characterization of some dielectric materials compatible with the 3D printing technique to study their dielectric characteristics and if they can be used to manufacture lens antennas.
- **Chapter 5** – This chapter describes the manufacture, measurement methods, and result analysis of the prototype antennas.
- **Chapter 6** – In the close chapter are the conclusions of the work developed and suggestions for future work.

1.4 Contributions

Some of the studies done throughout this dissertation provided the opportunity to publish a scientific article:

- V.Coelho, T.Varum, and J.N.Matos, "3D-Printed wide beamwidth lens antennas for beamforming coverage improvement", submitted and accepted for the 16th European Conference on Antennas and Propagation (2022 Edition of EuCAP)

CHAPTER 2

General concepts and state of the art

This chapter presents state of the art on lens antennas and intends to explain how they work and which techniques are best suited to fulfill the proposed objectives. Also, it is intended to understand which manufacturing techniques and construction materials are acceptable to fabricate lens antennas.

2.1 Lens antennas

The reflector antennas (such as dish antennas) are the most common method to change the radiation pattern. These reflector antennas reflect the signals to or from a source antenna (or feed antenna), allowing the modification of the radiation pattern. However, reflector antennas are a bit large compared to the feed and require some support for the source antenna, which can be complex or interfere with the operation of the antenna.

There is another type of antenna that can modify the radiation pattern: the lens antennas. Just as optical lenses deform light beams, lens antennas can change the beam propagation of RF waves. In lens antennas, the propagation of electromagnetic waves inside the lens is based on Snell's law, just as in optical lenses. The electromagnetic waves propagating inside the lens will be a refracted version of the incident wave. Therefore, the shape of the lens, the type of lens material, and the position of the source antenna relative to the lens body are factors that will influence the propagation of electromagnetic waves [1].

2.2 Classification of lens antennas

The shape, material, and the position of the source antenna relative to its body are all factors that influence the lens antenna's performance. So the classification of the lens antenna is based on these aspects [1].

2.2.1 Position of the source antenna

- **Off-Body Fed lenses** - when there is a physical separation between the source and lens antenna, so the electromagnetic waves propagate through the air between the source and the lens antenna (figure 2.1a). This separation affects the way the radiation beams focus on the lens[4].
- **Integrated lenses** - when the source and lens antenna are physically connected, electromagnetic waves propagate directly in the lens (figure 2.1b) [5].

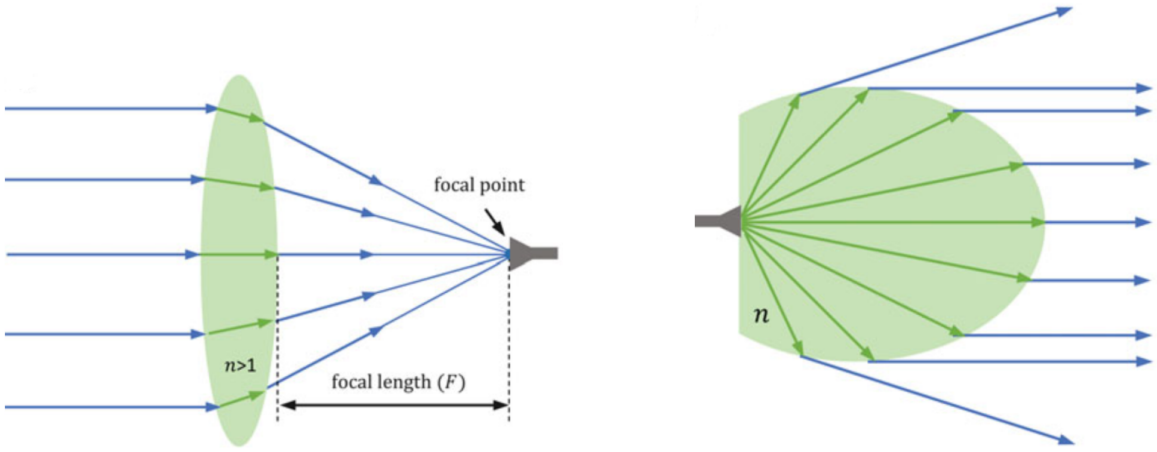

(a) Off-Body Fed lens antenna **(b)** Integrated lens antenna

Figure 2.1: Examples of lens antenna types (the green element represents the lens antenna body, and the grey element represents the source antenna) [1]

2.2.2 Lens antenna body materials

Most lens antennas are manufactured with dielectric materials, with a specific dielectric constant arranged inside the lens to have the desired effect on the propagation of the electromagnetic waves. So, there are homogeneous lens antennas made of a single material with a uniform dielectric constant throughout the lens body and lens antennas made of different dielectric constants that vary along the body, i.e., a multi-layer lens structure [6].

2.2.3 The physical shape of the lens body

Lens antennas can have various physical shapes ranging from simple elliptical and hyperbolic structures to more complex cylindrical and spherical forms. Figure 2.2 shows several examples of lenses.

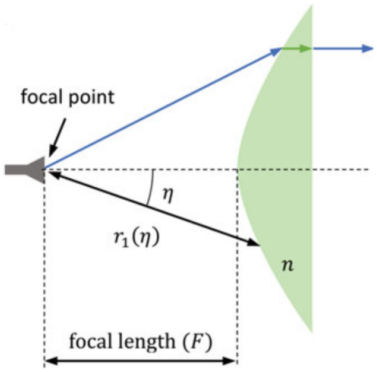

(a) Hyperbolic lens antenna (Off-Body Fed lens, homogeneous)

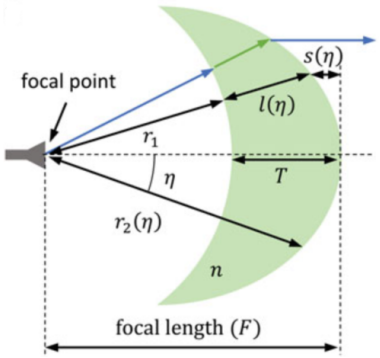

(b) Elliptical lens antenna (Off-Body Fed lens, homogeneous)

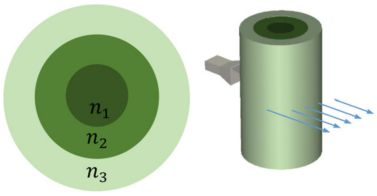

(c) Luneburg lens antenna (integrated multi-layer lens)

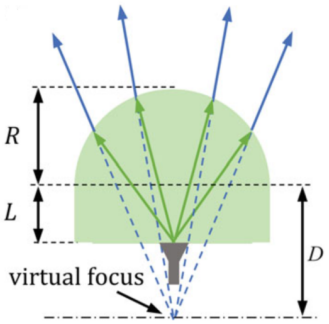

(d) Hyper-hemispherical lens antenna (integrated, homogeneous lens)

Figure 2.2: Examples of lens antenna structures (darker shades of green represent higher values of dielectric constants)[1]

2.3 Lens antennas as a study interest for this dissertation

Considering the objectives of this dissertation, multi-layer lenses present a greater versatility, so they can be analyzed to increase beamwidth. Of these, is the modified structure of the well-known Half Maxwell Fish-Eye (HMFE) structure, which will be extensively studied in this dissertation . Due to the complexity of these structures and the difficulty in understanding and simulating them, a more ordinary and simple structure will first be developed to understand better the electromagnetic simulator's, manufacturing techniques and measurement setup specifics.

2.3.1 Simple elliptical integrated lens antenna

The elliptical integrated lens is a structure with the source antenna integrated into its base, and it is made of a single material (single refracting surface) with the shape of a cut ellipsoid, as shown in figure 2.3a. Its design increases the directivity of the source antenna but with some limitations since it includes only one material with a single dielectric constant. Still, this directivity can be improved by inserting an outer layer with a different dielectric constant value (known as a matching layer). This layer will redirect the peripheral beams, focusing the antenna radiation even more and making a more directive antenna (figure 2.3b).

An Simple Elliptical Integrated (SEI) lens antenna design has the following parameter: dielectric constant (ε_r), the distance between the source antenna and the center of the lens (L) and the radius of the lens (small radius a and large radius b), the equation 2.1 [7] calculates those lens parameters. The value of the smallest radius of the lens a is responsible for the antenna directivity [1].

$$(\frac{x}{a})^2 + (\frac{y-L}{b})^2 = 1;\ b = \frac{a}{\sqrt{1 - \frac{1}{(\varepsilon_r)^2}}};\ L = \frac{b}{\varepsilon_r} \tag{2.1}$$

For the case of an integrated elliptical lens antenna with a matching layer, the dielectric constant (ε_{rmatch}) and thickness (h) of this match layer can be estimated using equation 2.2 where ε_{r1}, is the dielectric constant of the lens, ε_{rair} is the dielectric constant of the propagation medium (usually air) and λ_0 is the wavelength of the transmitted signal.

$$\varepsilon_{rmatch} = \sqrt{\varepsilon_{r1} \times \varepsilon_{rair}};\ h = \frac{\lambda_0}{4 \times \varepsilon_{rmatch}} \tag{2.2}$$

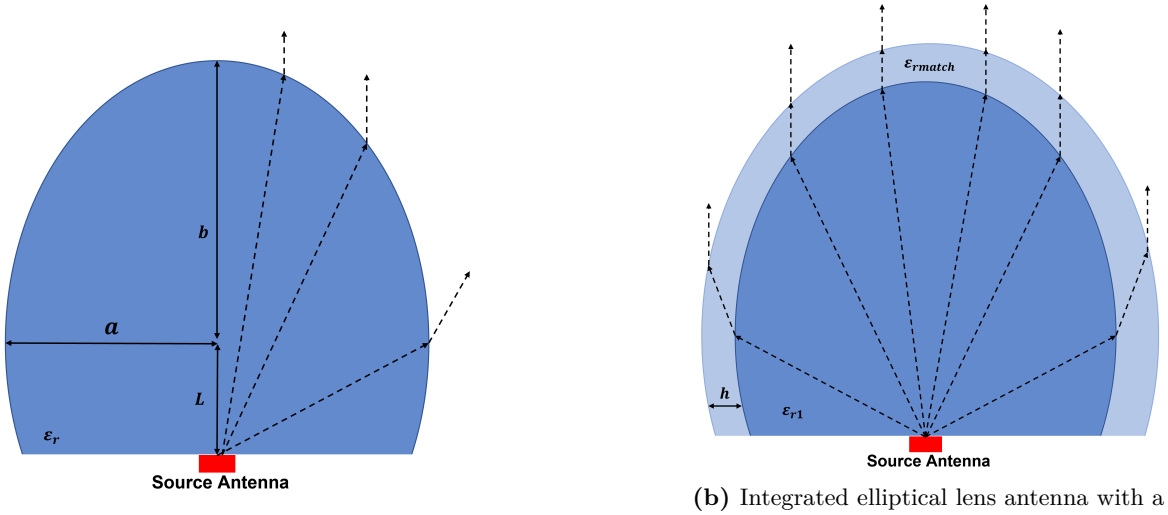

(a) SEI lens antenna

(b) Integrated elliptical lens antenna with a matching layer

Figure 2.3: Elliptical lens antenna

2.3.2 Half Maxwell fish-eye

The Maxwell Fish-Eye (MFE) lens antenna is a spherical integrated antenna with several layers with different dielectric constants, increasing along its radius from the center to the surface. Due to the body symmetry, placing a small source antenna its periphery, when the electromagnetic waves travel from the edge to the center of the lens, they will be transformed into planar waves, and from planar waves will converge into a focal point at the opposite end (figure 2.4) [8].

However, it may be more interesting to only have the conversion into planar waves. For this, use half of a sphere; this lens antenna is known as HMFE (figure 2.5a). The HMFE has the same operating principles and design as the MFE, with only half of the lens, because, in this way, it can get a planar wave from a source point (is a tiny source antenna compared to

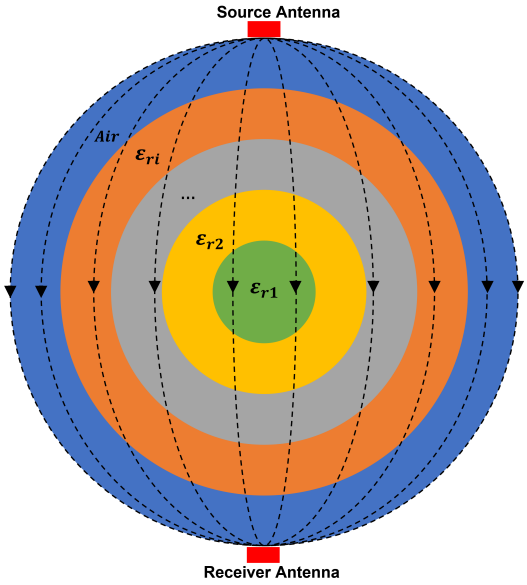

Figure 2.4: MFE lens antenna 2D view

the size of the lens antenna). When designing an HMFE, the only thing needed to know is the dielectric constant of each of the layers (ε_{ri}) of the semi-sphere that can be estimated through the equation 2.3 [9], where r_i is the radius of the layer in question, and D is the diameter of the semi-sphere (figure 2.5b).

$$\varepsilon_{ri} = \frac{4}{(1 + (2 \times (\frac{r_i}{D})^2))^2} \tag{2.3}$$

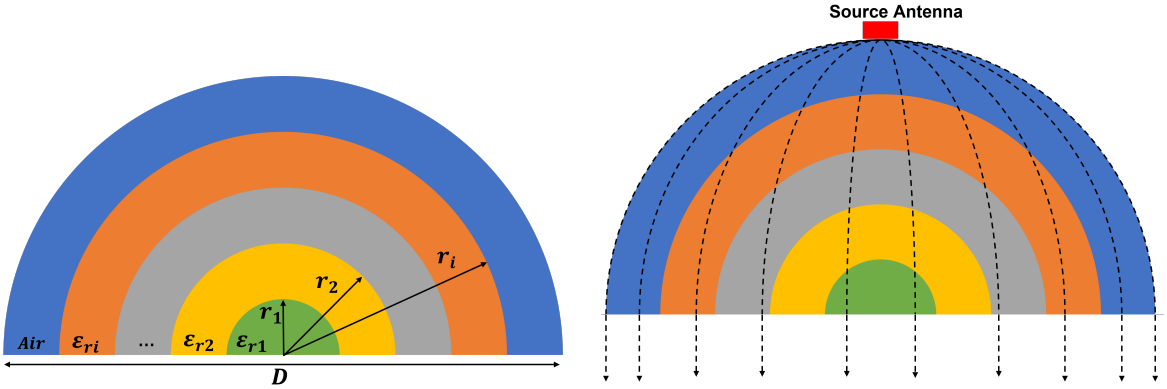

(a) Distribution of layers of different dielectric constant

(b) Propagation of electromagnetic waves inside the lens

Figure 2.5: Traditional HMFE Lens Antenna 2D view

2.3.3 Modified structure of a Half Maxwell fish-eye

The MHMFE is an integrated multi-layer lens antenna proposed in an article published [2] in the *IEEE Antennas and Propagation Society International Symposium* by researchers Zixuan Yi and Qi Zhu. This new model of lens antenna is based on HMFE.

The MHMFE has a modified geometry alteration of the HMFE, obtained by dividing the half-circle of the HMFE (figure 2.5) into two-quarters and reversing its positions (figure 2.6). The whole MHMFE structure is obtained by rotating these two-quarter circles around their union point (figure 2.6). This lens has multiple layers, and the most peripheral layer has a dielectric constant value of 1, which corresponds to the air. The lowest layer (layer 1 in figure 2.7) has the highest dielectric constant value (less than 4), and the remaining layers fall between these values. the calculation of each layer radius is performed using the equation 2.4, where D is the diameter of the lens, r_i is the radius of each layer, and ε_{ri} is the dielectric constant of each layer.

$$r_i = D \times \sqrt{\frac{\sqrt{\frac{4}{\varepsilon_{ri}}} - 1}{2}} \tag{2.4}$$

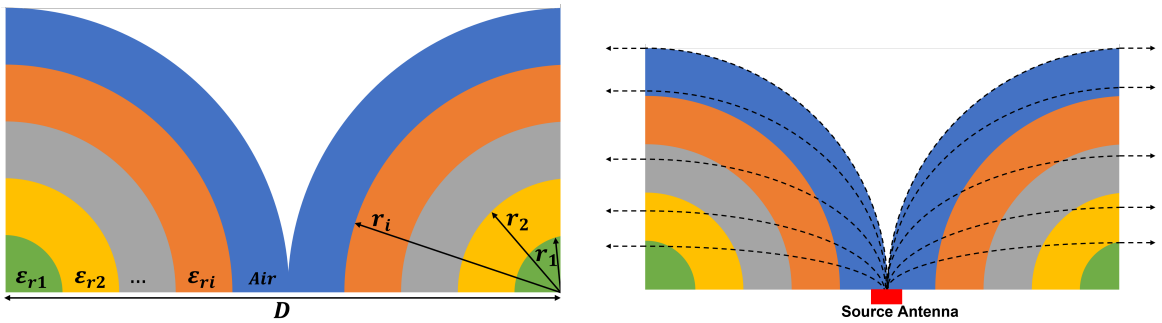

(a) Distribution of layers of different dielectric constant

(b) Propagation of electromagnetic waves inside the lens

Figure 2.6: MHMFE lens antenna 2D view

This MHMFE structure increases the HPBW of a source antenna, as suggested in [2], where it was possible to obtain a beamwidth of 160° from a microstrip patch. The dimensions of this structure (diameter, layer radius, and height (H)) have to be adjusted to obtain a lens optimized for each case.

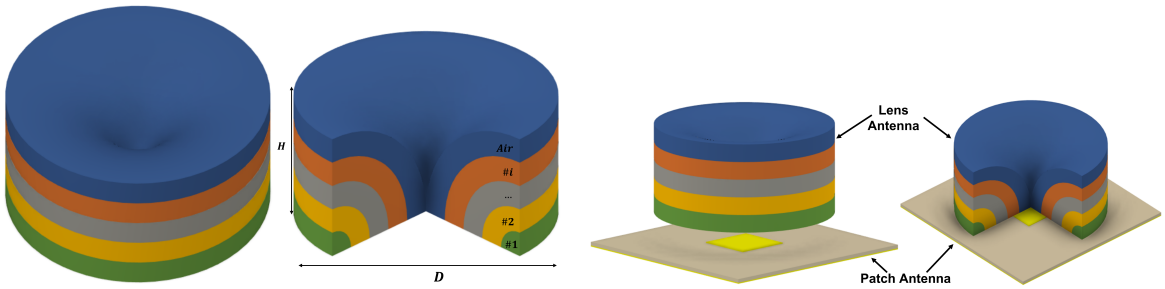

(a) MHMFE 3D view

(b) MHMFE lens antenna and patch antenna

Figure 2.7: MHMFE lens antenna 3D view

2.4 Manufacture of lens antennas

There are several ways to manufacture lens antennas, depending on the lens's type, shape, and materials. Though, the most common manufacturing methods are injection manufacturing

(with molds), subtractive manufacturing (using Computer Numerical Control (CNC)), and additive manufacturing (3D printers) (figure 2.8). All these methods have their advantages and disadvantages for the manufacture of lens antennas [10].

(a) Molding technique **(b)** Subtractive manufacturing

Figure 2.8: Examples of manufacturing methods [1]

The most exciting technique for manufacturing lens antennas is additive manufacturing, or, as it is commonly known, 3D printing. This manufacturing technique is a low-cost method for manufacturing parts in small quantities, as in prototyping, and allows the manufacture of unique parts made of various materials inter-linked and parts with the most varied shapes. However, the term 3D printing covers various types of additive manufacturing the *ISO/ASTM 52900 Standard* [11], considers the existence of seven technologies (figure 2.9) [12].

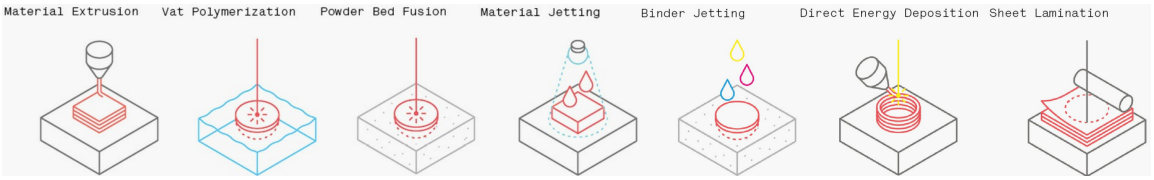

Figure 2.9: Additive manufacturing technologies [12]

Material extrusion is a manufacturing method that dispenses the molten material through an orifice (known as a nozzle). All the printers in Instituto de Telecomunicações (IT) use this manufacturing method, specifically the Fused Deposition Modeling (FDM) technology. The build material comes in filament rolls, which are fed into a heated extruder that melts the material and passes it through a nozzle, depositing it in layers to obtain the desired part [12]. Considering this, some parameters influence both the physical structure and the dielectric properties:

- **Material** - The material is the first thing to consider when making a part, as it dictates the main characteristics of the print (such as extruder temperature) and the part.
- **Layer height** - As the name implies, this is the height of each layer of material deposited. This height is primarily influenced by the size of the nozzle used and must be smaller than the size of the nozzle (e.g., for a 0.4mm nozzle, the ideal layer height is around 0.2/0.3mm) [13].

- **Thickness/number of the top and bottom layers** - The base layer is crucial because it makes adhesion between the construction base and the part, while the top layer ensures its integrity. The thickness of these layers is a multiple of the layer height, i.e., two base/top layers have a thickness equivalent to twice the layer height.
- **Thickness/number of the outer shell** - The walls are, as the name implies, the most peripheral part of the part between the top and bottom, the nozzle size dictates the thickness [14].
- **Infill** - The infill is the part between the outer shell, base, and top. It is usually neither totally filled nor empty, so it is filled with a percentage of material arranged in a predefined pattern (rectangular, triangular, honeycomb, and many others) [15].

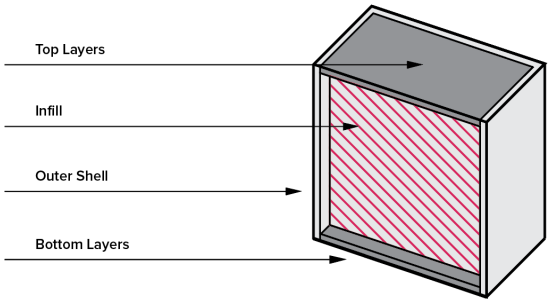

Figure 2.10: Diagram of an FDM manufactured part [16]

There are two available printers for use: the Creality Ender 3 (CE3) (personal) and the Ultimaker 3 Extended (UM3E) (from IT). They are both virtually similar, working the same way, with a difference in filament gauge used (1.75mm for CE3 and 2.85mm for UM3E). However, the UM3E allows printing on two different materials simultaneously.

2.5 Use of dielectric materials in lens antennas

Dielectric materials can be considered insulating materials, i.e., they have high electrical resistivity. However, when exposed to a sufficiently high external electric field allows some electric current flow [17]. There are several types of dielectric materials such as air, porcelain, glass, and plastics. For the intended application, the most interesting are the plastic polymers compatible with FDM. Table 2.1 shows a list of the most popular dielectric filaments in FDM (Nylon, Polyethylene Terephthalate Glycol (PETG) and Polylactic Acid (PLA)) and some of their electrical properties. Still, these values are not precise because the filament dielectric characteristics depend on their color [18], manufacturer, or even the characteristics of the 3D printing (such as the spacing of layers [19], the amount and shape of the infill [20], amount of material used [21], among others [22]). These various degrees of freedom mean that it is more appropriate to measure the materials to obtain dielectric constant and loss tangent values [23].

Table 2.1: Electrical properties of some filaments (values for 1MHz)

Filament	Dielectric constant	Loss Tangent
Nylon	3.24 [24]	0.037 [24]
Polyethylene Terephthalate Glycol (PETG)	2.40 [25]	0.02 [25]
Polylactic Acid (PLA)	2.70 [26]	0.008 [26]

2.5.1 Measurement of the dielectric constant of dielectric materials

As previously mentioned, several parameters can affect the dielectric constant of a given material, in this case, of a part manufactured by FDM. To manufacture the intended lens structure, it requires some precision in the value of the dielectric constant of the material used, and it was decided to perform measurements to characterize and estimate the dielectric constant of the available materials.

There are several methods for doing this type of material characterization, such as resonant and non-resonant methods [27] [28]. However, some of these characterization methods can be too complex (specialized techniques/equipment required, several material samples). Therefore, the Single Microstrip Line Characterization (SMLC) method [29] was chosen, which is a more straightforward method than those previously mentioned, requiring only a sample of the material to be characterized, with a conductive line and ground plane (copper tape) placed over it, and a Vector Network Analyzer (VNA) to measure the resonance frequency of the material. A detailed description of how to characterize materials with the SMLC method can be found in appendix A.

2.6 Microstrip patch antennas

The lens antennas are always associated with another traditional antenna, the source antenna responsible for emitting/receiving the signal. In this case, the most suitable antenna to test this concept is the microstrip patch antenna, which is extremely easy to design and manufacture, is very versatile, and has a beamwidth of 60°/70°.

2.6.1 Shape

A patch antenna is a type of microstrip antenna with a reduced profile compared to other antennas. This type of antenna usually has a structure similar to the one shown in figure 2.11. Comprising of a ground plane, a substrate, and a radiating element called the patch, where the ground plane and the patch are made of a conductive material (copper) and the substrate of a dielectric material.

The patch structure can have several shapes influencing the radiation pattern's shape, antenna polarization, and antenna gain. The most common shapes are the rectangular patch and the circular patch, and these patch shapes provide Linear Polarization (LP).

The design of a rectangular patch involves discovering two main dimensions (figure 2.11): the length (W_{patch}) and the width (L_{patch}). The following formulas allow calculating those dimensions. ε_r is the dielectric constant of the substrate, f_r is the resonance frequency of the

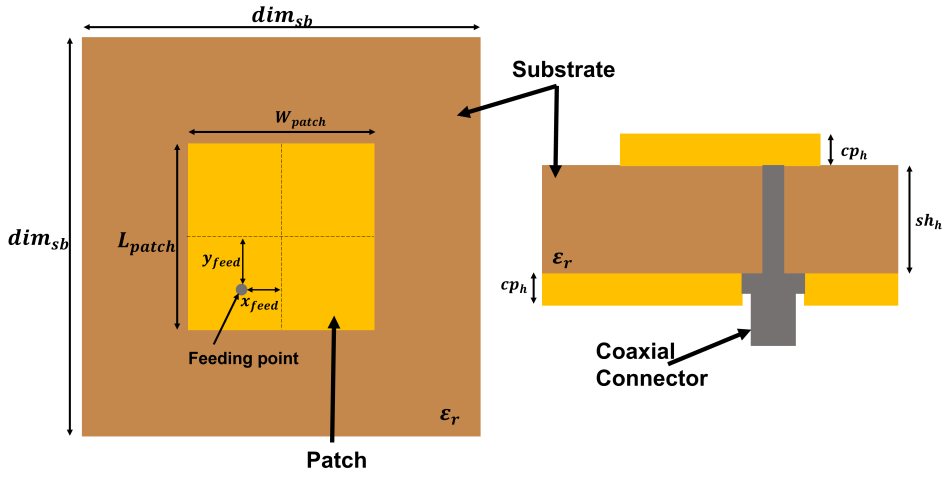

Figure 2.11: Diagram of the rectangular patch antenna

antenna, sb_h the thickness of the substrate, ε_{reef} is the effective dielectric constant, and c is the speed of light [30].

$$
\begin{aligned}
W_{patch} &= \frac{c}{2f_r} \times \sqrt{\frac{2}{\varepsilon_r + 1}} \\
\varepsilon_{reef} &= \frac{\varepsilon_r + 1}{2} \times \frac{\varepsilon_r - 1}{2} \times \frac{1}{\sqrt{1 + 12 \times \frac{sb_h}{W_{patch}}}} \\
\Delta L_{patch} &= 0.412 sb_h \times \frac{(\varepsilon_{reef} + 0.3)(\frac{W_{patch}}{sb_h} + 0.264)}{(\varepsilon_{reef} - 0.258)(\frac{W_{patch}}{sb_h} + 0.8)} \\
L_{patch} &= \frac{c}{2f_r\sqrt{\varepsilon_{reef}}} - 2\Delta L
\end{aligned}
\tag{2.5}
$$

When designing a circular patch, it is enough to calculate the radius of the microstrip circle (a_{patch}), taking into account with the same parameters as before, the equation 2.6 [30] can be used to determine this value .

$$
\begin{aligned}
a_{patch} &= \frac{F}{\sqrt{1 + \frac{2 \times sb_h}{\pi \times \varepsilon_r \times F} \times (\ln \frac{\pi \times F}{2 \times sb_h} + 1.7726)}} \\
F &= \frac{8.791 \times 10^9}{f_r \times \sqrt{\varepsilon_r}}
\end{aligned}
\tag{2.6}
$$

2.6.2 RF signal feed

A fundamental feature of these antennas is the feed, which can be done in several ways depending on the patch format and application. However, the Microstrip line feed and probe/coaxial feed are the most used. The Microstrip line feed consists of a line extending from the edge of the substrate to the patch. This line's width and length must be adjusted to allow the best matching antenna impedance. The probe feed method uses a coaxial connector or cable directly connected through a hole drilled from the patch to the ground plane (the position of this feed point determines the impedance matching between the system and antenna).

2.6.3 Antenna polarization

Usually, patch antennas have LP. However, to have a different polarization, such as Circular Polarization (CP), it is enough to change the shape of the patch or position the feed in a strategic position. Figure 2.12a shows an example of a square patch antenna with CP. This antenna is an adaptation of a square patch antenna $W = L$ in which two of the corners of the squares are cut off. These cuts are associated with the position of the feed, which makes the antenna have a CP. So with the structure of figure 2.12a, if the feed is at the point indicated as feeding point 2, we have Right Hand Circular Polarization (RHCP), and if it is at feeding point 1, we have Left Hand Circular Polarization (LHCP) [30] [31].

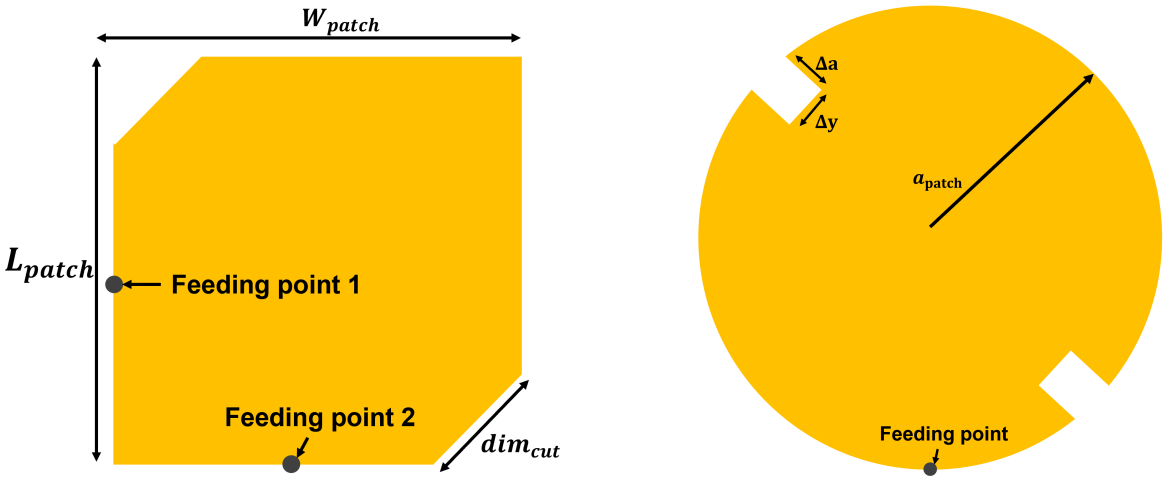

(a) Square patch antenna with CP

(b) Circular patch antenna with CP

Figure 2.12: Examples of patch antennas with circular polarization

In figure 2.12b, there is another example of an antenna with CP, in this case, a circular patch antenna with two cutouts on the diagonal of the circumference with a given opening (Δy) and depth (Δa). The position of these cutouts will define the direction of circular polarization. For example, if the cutouts and feed are in the positions indicated in figure 2.12b, the antenna will have LHCP [32].

CHAPTER 3

Simulation of antenna lens

This chapter analyzes lens antenna structures using simulations to understand if they work as indicated in state-of-the-art and if it is possible to fabricate using 3D printing.

3.1 Simulation process

3.1.1 Simulation tool

The simulation of lens antennas requires specialized software, so it was considered to use different tools, more precisely, the *CST Studio Suite* [33] or *ILASH* [34]. The *ILASH* is a tool developed by colleagues from the IT from other universities and allows the design, analysis and optimization of integrated lens antennas. However, it only allows very limited simulations, for example, it only allows simulations of lenses with one or two layers with the circular and symmetrical geometry, and it also does not have much freedom in the design of the source antenna, which is a bit limiting for the intended application.

The ultimate goal is to develop a multi-layer antenna, and the simulator that meets these requirements is the *CST Studio Suite*. This tool allows the creation of lenses with several layers and geometric shapes, designing the source antenna with the desired specifications, and a more extensive and rigorous analysis of the results obtained. For this reason, the *CST Studio Suite* was the tool used in all simulations

3.1.2 Source antenna

It is essential to design a good source antenna when simulating lens antennas because this influences their performance. Therefore, the source antenna will be a patch antenna with a resonance frequency of 7.8GHz, LP square patch, and coaxial feed. This antenna is simple to design and manufacture with reasonable dimensions and has the potential to increase the HPBW. Furthermore, the coaxial feed method makes the antenna less influenced by the lens structure than other feeding methods, such as the Microstrip Line Feed method.

This patch antenna used a *Rogers RO4725JXR* substrate (with a dielectric constant of 2.55, height 0.78mm, and copper height 0.018mm), a square shape, and dimensions calibrated

for the desired resonance frequency. As the simulations and testing progressed, the antenna dimensions were updated to keep the resonance frequency at 7.8GHz with a good impedance matching.

3.2 Single Elliptical Integrated lens Antenna

The main objective of simulating the SEI lens antenna is to ensure that the *CST Studio Suite* allows this kind of simulation and learn how to use the simulator and analyze the results.

Designing an SEI lens antenna is simple. It is just a matter of calculating the three main parameters (small radius a, large radius b and the position of the source antenna relative to the antenna center L) with equation 2.1. Table 3.1 shows the antenna parameters for three different cases. This type of lens antenna increases the directivity of the source antenna, and this directivity can be adjusted with the small radius (a). Therefore, with these three different cases, it is expected that each one of them will have a different directivity level than is higher than in the case without the lens.

In *CST Studio Suite*, there is no direct method to draw an ellipsoid, but it can be created by deforming a sphere using the process described in appendix B.

Table 3.1: SEI antenna lens parameters

SEI lens antenna	
Lens dielectric constant $\varepsilon_r = 2$	
Case 1	$a = 20mm$ $b = 23.09mm$ $L = 11.55mm$
Case 2	$a = 30mm$ $b = 34.64mm$ $L = 17.32mm$
Case 3	$a = 40mm$ $b = 46.19mm$ $L = 23.09mm$
Patch antenna	
Total area	$100mm \times 100mm$
Patch dimensions	$10.496mm \times 10.496mm$

3.2.1 Simulation results

The results (figure 3.1) show that increasing the small radius (a) of the lens antenna the main lobe tends become narrower (reduce the beamwidth). Thus the antenna is more directive, and these are the expected results for an SEI lens antenna. A side effect of this antenna is the appearance of the secondary lobes alongside the main lobe. This effect is due to the SEI lens antenna having difficulties compensating for side beams. The integrated elliptical lens antenna with a matching layer solves this problem as the matching layer can help reduce these secondary lobes because it redirects the side beams in the direction of interest.

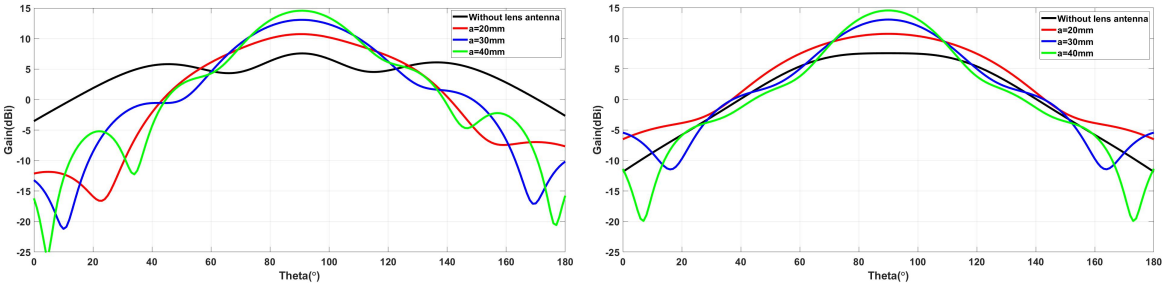

(a) Radiation pattern for $\phi = 0°$ **(b)** Radiation pattern for $\phi = 90°$

Figure 3.1: Simulation results of the SEI lens antenna using a patch antenna as source

3.3 Simulation of the Modified Half Maxwell fish-eye lens Antenna

The design of an MHMFE is constructed iteratively, i.e., layer by layer starting with the largest radius layer (assuming the example of a 10-layer lens starting with layer 10), following the steps in appendix C.

3.3.1 Simulation results

The figure 3.2 shows the results of using an MHMFE lens with different diameters (table 3.2, height of $H = \frac{D}{2}$). Increasing the lens antenna's diameter leads to the appearance of two side lobes with a valley between them. This effect is not desirable because it does not make the antenna gain uniform across the entire beamwidth. Varying the height ($H = 0.1 \times \lambda_0 = 3.85$, $H = 0.3 \times \lambda_0 = 11.55$ and $H = 0.5 \times \lambda_0 = 19.25$) of the lens antenna does not significantly improve this problem, as shown in the figure 3.3 (in this case the diameter of lens was $D = 1.2 \times \lambda_0 = 46.20$).

Table 3.2: Radius of the MHMFE lens antenna layers

$D(mm)$	r_1	r_2	r_3	r_4	r_5	r_6	r_7	r_8	r_9	r_{10}
$1.0 \times \lambda_0$ 38.50	2.39	5.65	7.24	8.8	10.43	12.02	13.66	15.25	16.87	18.42
$1.1 \times \lambda_0$ 42.35	2.62	6.22	7.96	9.71	11.48	13.23	15.02	16.78	18.55	20.26
$1.2 \times \lambda_0$ 46.20	2.86	6.78	8.69	10.59	12.52	14.42	16.38	18.30	20.24	22.10
$1.5 \times \lambda_0$ 57.75	3.58	8.48	10.86	13.25	15.65	18.04	20.49	22.875	25.30	27.63

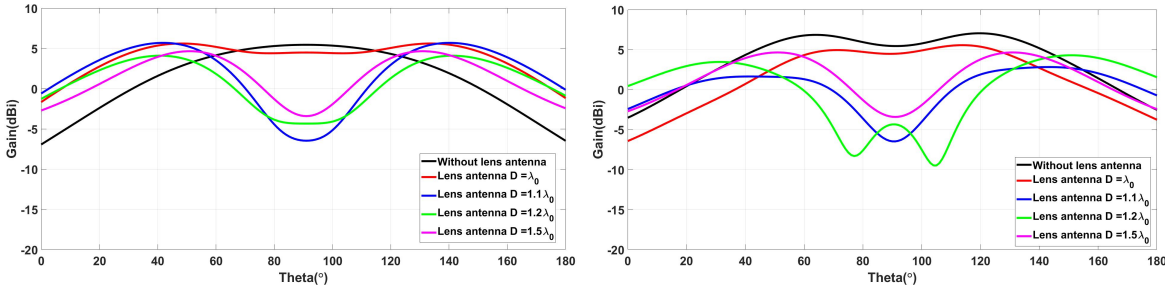

(a) Radiation pattern for $\phi = 0°$ **(b)** Radiation pattern for $\phi = 90°$

Figure 3.2: Simulation results of MHMFE lens antenna using patch antenna for different lens diameters

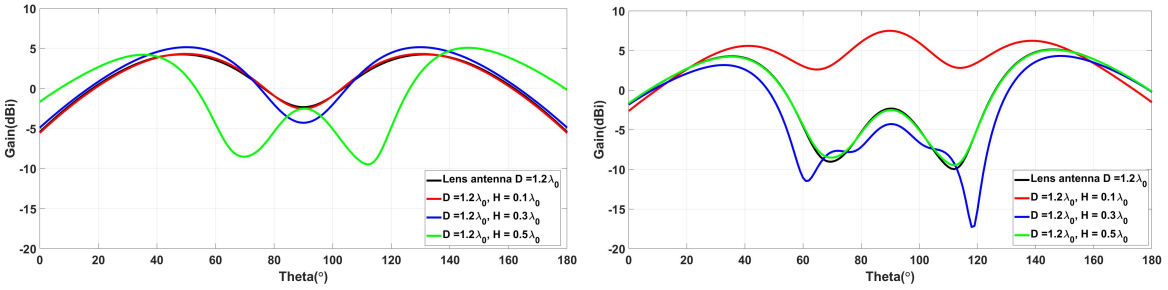

(a) Radiation pattern for $\phi = 0°$ **(b)** Radiation pattern for $\phi = 90°$

Figure 3.3: Simulation results of MHMFE lens antenna using patch antenna for different lens heights

Another possible variation on the lens body is the layers' dielectric constant values, which will also vary the radius of the layers. These layers should have a dielectric constant starting at a higher value (less than 4) and ending close to 1 (air). Therefore, where simulated three possible cases (table 3.3) with a different dielectric constant (for lens diameter of 100mm).

In figure 3.4, the radiation pattern tends towards better results for lower dielectric constant values, such as case 3. However, those low dielectric constant values lead to a small spacing between the last layers (approximately 1mm for the first layers). These tiny distances are not an ideal situation.

Table 3.3: Layer radius of MHMFE lens antennas for different dielectric constant values

Layer	$i=1$	$i=2$	$i=3$	$i=4$	$i=5$	$i=6$	$i=7$	$i=8$	$i=9$	$i=10$
Case 1										
ε_{ri}	3.88	3.39	3.07	2.73	2.39	2.07	1.77	1.51	1.28	1.09
$r_i(mm)$	6.19	14.68	18.81	22.94	27.1	31.23	35.47	39.61	43.81	47.84
Case 2										
ε_{ri}	2.8	2.61	2.42	2.23	2.04	1.85	1.66	1.47	1.28	1.09
$r_i(mm)$	22.09	24.39	26.72	29.12	31.63	34.29	37.16	40.3	43.81	47.84
Case 3										
ε_{ri}	1.8	1.72	1.64	1.56	1.48	1.41	1.33	1.25	1.17	1.09
$r_i(mm)$	35.03	36.21	37.44	38.72	40.05	41.44	42.91	44.45	46.09	47.84

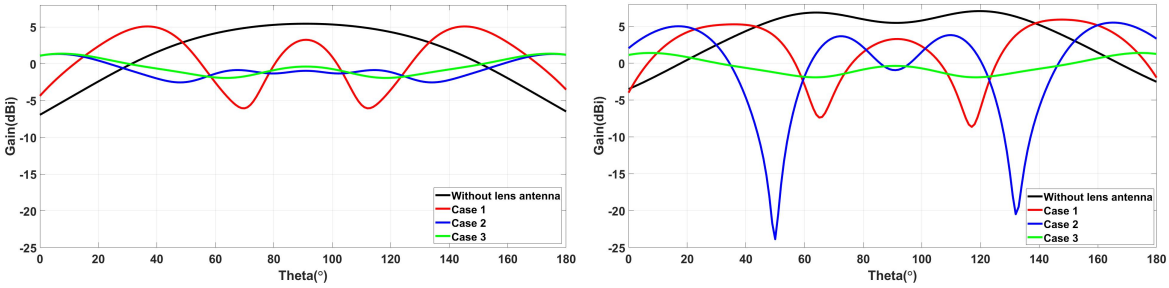

(a) Radiation pattern for $\phi = 0°$ **(b)** Radiation pattern for $\phi = 90°$

Figure 3.4: Simulation results of the MHMFE lens antenna using the patch antenna as a source, using the dielectric constants in table 3.3

For this reason, the relationship between the dielectric constant and the layers' radius was ignored to obtain better results and structures. Thus, the lens antenna were redesigned (assigning an acceptable layers radius and reducing the number of layers to five), also the patch antenna was recalibrated for this new lens antenna.

After several tests, the best results were achieved using 5-layer lens antennas with the dimensions described in table 3.4 and the results of figures 3.5 and 3.6. Compared to the case without a lens, the radiation HPBW increases significantly, in the plane $\phi = 0°$ from 66° (without lens) to 128° (with lens) and in the plane $\phi = 90°$ increases from 60° (without lens) to 168° (with lens). Despite not obtaining the promised beamwidth greater than 160° in both planes (vertical and horizontal), the results are satisfactory. This discrepancy is caused by the different behavior of each plane when interacting with the lens. After the characterization of the dielectric materials, the simulations must be redone, considering the materials' dielectric constants.

Table 3.4: Parameters of the MHMFE lens antenna for the best case

5-Layer Lens					
Layer	1	2	3	4	5
Dielectric constant	1.9	1.675	1.45	1.225	1
Layer radius (mm)	10	20	30	40	50
Lens diameter	100mm				
Patch antenna					
Total area	$100mm \times 100mm$				
Patch dimensions	$11.11mm \times 11.11mm$				

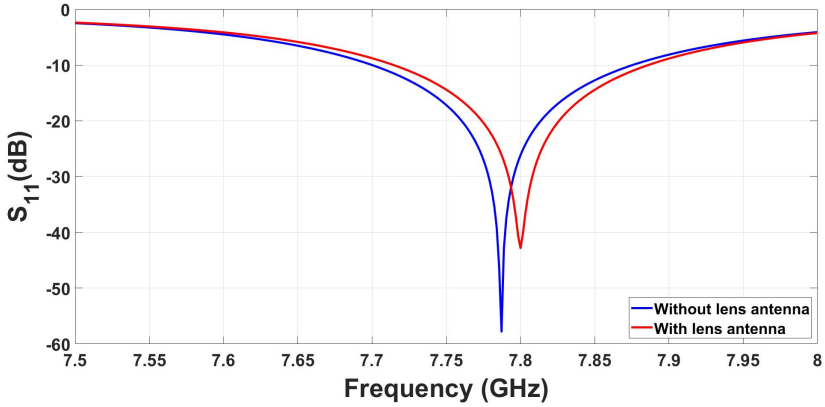

Figure 3.5: Reflection coefficient of the 5-layer MHMFE lens antenna

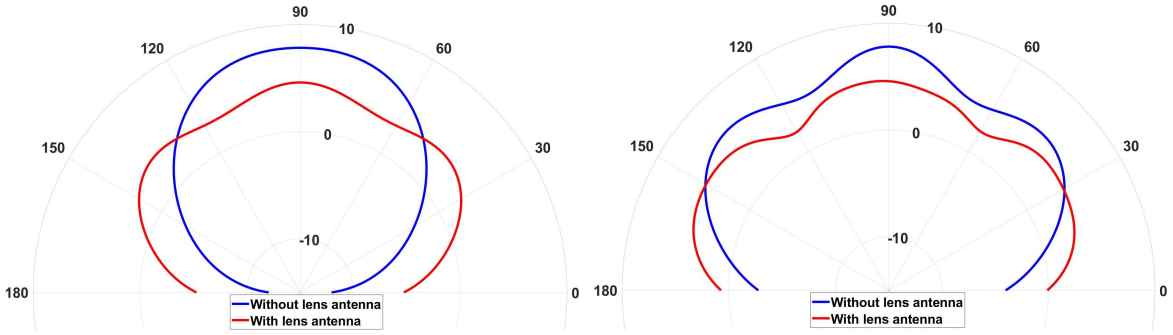

(a) Radiation pattern for $\phi = 0^\circ$ **(b)** Radiation pattern for $\phi = 90^\circ$

Figure 3.6: Radiation pattern of the 5-layer MHMFE lens antenna

CHAPTER 4

Characterization of dielectric materials

This chapter presents the characterization of some dielectric materials compatible with the 3D printing technique to study their dielectric characteristics and if they can be used to manufacture lens antennas.

4.1 Results of characterization of known materials (*Rogers RO4725JXR*)

Before starting to characterize 3D printed materials with unknown characteristics, the SMLC method should be evaluated for its effectiveness. For this, was characterized a substrate with well-described characteristics, the *Rogers RO4725JXR*. Three different samples (with a certain length L, width W_s, height h and line width W_l) were put under test (table 4.1.), assessing the conditions $\frac{W_l}{h} \leq 1$ and $\frac{W_l}{h} > 1$ and the case of different sample widths.

The manufacture datasheet claims that the *Rogers RO4725JXR* with a substrate thickness of $h = 0.78mm$, dielectric constant of $\varepsilon_r = 2.55$, and loss tangent of $\tan(\delta) = 0.0026$ (values for 10GHz) [35]. The table 4.1 shows the dielectric constant and loss tangent values obtained by the SMLC method. For the case of $\frac{W_l}{h} > 1$ (Samples 1 and 3) the dielectric constant values are relatively close to the datasheet value. However, in the case of $\frac{W_l}{h} \leq 1$ (Sample 2), there is a considerable discrepancy. All the loss tangent values have considerable differences and are not plausible. Therefore, to determine the dielectric constant, it is better to have samples for the case of $\frac{W_l}{h} > 1$, for more realistic dielectric constant values, and due to the significant discrepancies in the loss tangent values, it will be better to consider the datasheet values.

Table 4.1: Characterisation of Rogers RO4725JXR samples

Samples	**L (mm)**	W_s **(mm)**	W_l **(mm)**	ε_r	$\tan(\delta)$
Sample 1	20	40	1	2.10	0.087
Sample 2	20	25	0.7	4.69	0.071
Sample 3	20	25	1	2.32	1.78

4.2 Results of the characterization of 3D printed materials

Were characterized three common materials for manufacturing with 3D printing PLA, PETG, and nylon. This study requires the test of several samples (figure 4.1) of each material with different infill and wall thicknesses (for PLA and PETG only) to understand how the material's dielectric constant varies with the amount of material in the parts. Table 4.2 shows the dielectric constant for several 3D samples. These values are within the expected range and are similar to datasheet values (table 2.1). As the material volumetric percentage decreases, the dielectric constant also decreases due to the increased percentage of air in the sample. However, the dielectric constant does not drop much beyond 1.8 because the volumetric percentage of material cannot be reduced below 16% because the sample becomes too fragile and unviable to manufacture structures. A more detailed analysis of the results acquired can be seen in appendix D.

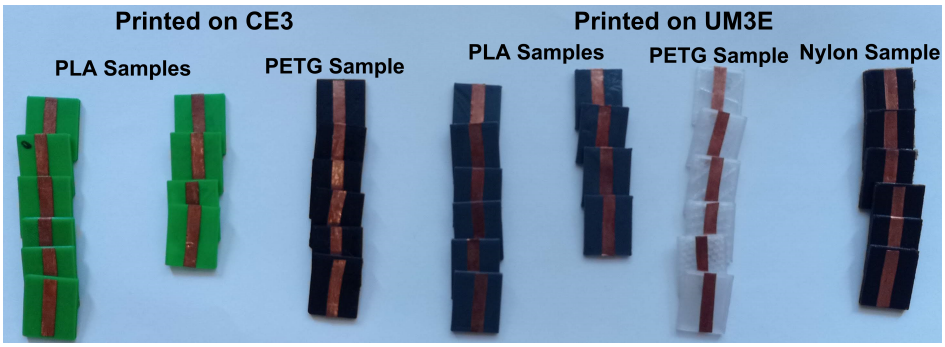

Figure 4.1: Material samples for characterization

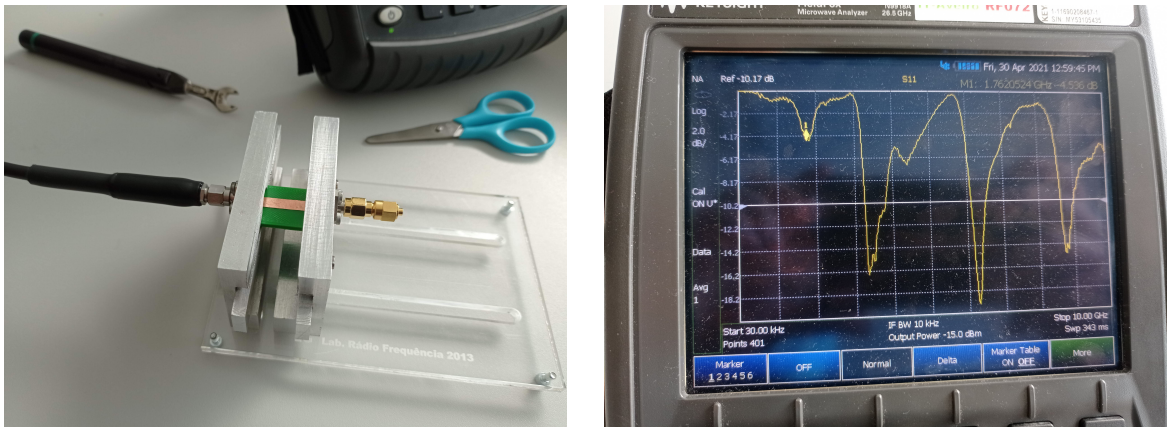

(a) Setup for measuring the samples **(b)** Example of sample measurement in the VNA

Figure 4.2: Setup for measuring the samples

Table 4.2: Characterisation of the 3D printed samples

Printer	Material	Infill	ε_r
Creality Ender 3	**PLA**	0%	1.92
		10%	1.96
		20%	2.31
		35%	2.13
		50%	2.18
		100%	2.79
		0% - Thin walls	1.85
		10% - Thin walls	2.07
		20% - Thin walls	2.07
		30% - Thin walls	2.29
	PETG	0%	2.10
		10%	2.11
		20%	2.25
		35%	2.25
		50%	2.28
		100%	2.50
Ultimaker 3 Extended	**PLA**	0%	2.10
		10%	2.14
		20%	2.15
		35%	2.27
		50%	2.25
		100%	2.63
		0% - Thin walls	1.95
		10% - Thin walls	2.01
		20% - Thin walls	2.06
		30% - Thin walls	2.26
	PETG	0%	2.14
		10%	2.20
		20%	2.28
		35%	2.35
		50%	2.35
		100%	2.71
	Nylon	0%	2.65
		10%	2.49
		20%	2.84
		35%	2.72
		50%	2.73
		100%	3.34

CHAPTER 5

Prototypes and experimental measurements

This chapter describes the manufacture, measurement methods, and result analysis of the prototype antennas.

5.1 Prototype antennas

From the simulation results in chapter 3 and the characterization results (chapter 4), it is noticeable that the initially designed antennas are not feasible with the available materials, so the lens antennas must be redesigned to be fabricated with the available materials. In addition, the patch antennas also have to undergo some minor changes to accommodate a 50Ω SubMiniature version A (SMA) connector.

A prototype SEI lens antenna (figure 5.1) was fabricated (to test the fabrication technique and measurement setup for a more straightforward design). In the case of the MHMFE lens antenna, several prototypes were fabricated in two different ways:

- **Single material lens antennas** - the entire lens is made of the same material, varying the infill of each layer to obtain different dielectric constants. Two samples of 5, 4, and 3-layer lens antennas were made. Both samples are identical, just changing the material and printer used (one on the CE3 printer with Tucab PLA Green filament, and the other on the UM3E printer Filamentive PLA Grey). Each set of samples has a patch antenna for feeding. For simplicity, the lens antennas will be called by the name of the printer where they were manufactured (figure 5.2a).
- **Multi-material lens antennas** - the lens manufactured using different solid materials for each layer. Due to material limitations, manufacturing was only possible for the lenses with a 4-layer (Nylon, PETG, and PLA) and a 3-layer (Nylon and PETG) on the UM3E printer. Each antenna lens has three possible choices of patch antenna (LP square patch, CP square patch (figure 5.2b), and CP circular patch (figure 5.17)).

The topmost layer of all lens antennas corresponds to an air layer, included in the simulation but not physically printed.

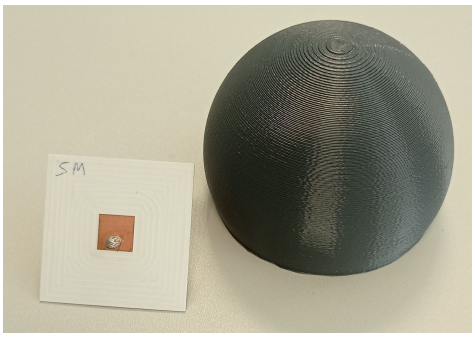

Figure 5.1: SEI Lens antenna prototype

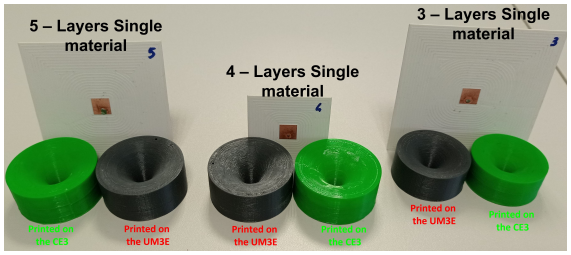

(a) Single material lens antennas and patch antennas

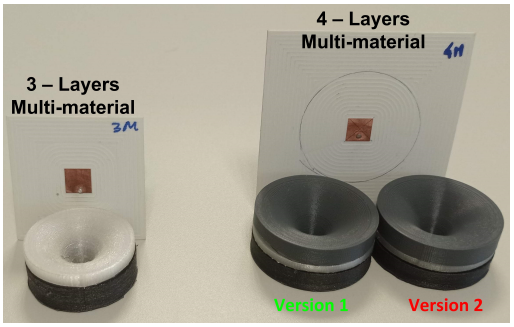

(b) Multi-material lens antennas and patch antennas

Figure 5.2: MHMFE Lens antennas prototypes

5.2 Measurement setup

To evaluate the performance of the manufactured antennas, it is necessary to measure some parameters such as reflection coefficient, impedance, and radiation pattern to compare them with the values obtained by simulation. The reflection coefficient and impedance of the antenna can be measured using any VNA. However, to measure the radiation pattern, it is necessary to measure the antennas in an anechoic chamber using two antennas (the antenna under test and a standard antenna) where the antenna under test has to be rotated 180° in the horizontal direction, and the S_{21} parameter is measured using a VNA. In the University of Aveiro, there are two anechoic chambers available for use (one in the Departamento de Eletrónica, Telecomunicações e Informática (DETI) (figure 5.3b) and other on the IT (figure 5.3a)), unfortunately, the measurement equipment is inoperative in both. For that reason, a measurement setup for the anechoic chamber of the IT was improvised.

The improvised measurement setup was built using: a stepper motor, a motor controller, Arduino to rotate the antenna under test, and a VNA (*Keysight FieldFox N9918A*) to measure the S_{21} parameter. In the anechoic chamber, the test antenna and standard antenna are separated at a distance greater than the farfield distance, with the standard antenna mounted

in a fixed position and the antenna under test mounted on the stepper motor so that it can be rotated (both antennas must be level and aligned).

The whole measurement system is controlled by a computer, which sends commands to an Arduino, through a serial port, to rotate the stepper motor (about 9° per iteration from 0° to 180°) and communicates via local area network with the VNA *Keysight FieldFox N9918A* (the VNA's communication code is based on the one provided by the manufacturer [36]). Each measurement's sequence returns the radiation pattern and a text file with this data.

This semi-automatic measurement setup allows for better repeatability and accuracy than a manual method of rotating the antenna manually for each measurement (it also allows faster and more efficient acquisition). However, it still has a very high measurement error due to setup problems. As the work progressed, this setup proved to be too unstable for more precise measurements, so the DETI anechoic chamber was used because it already has a more sophisticated measurement setup.

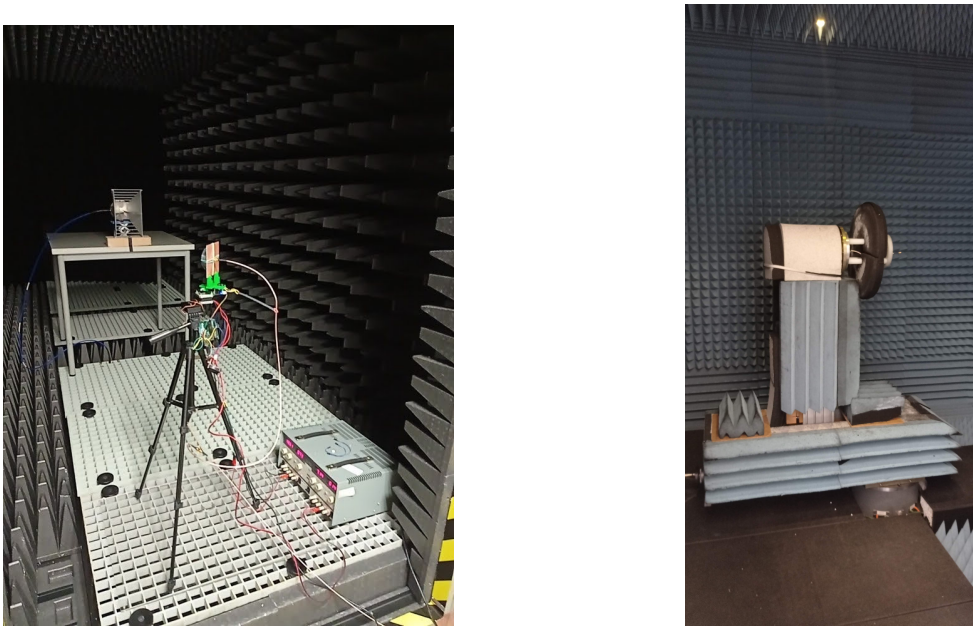

(a) Measurement Setup in IT **(b)** Measurement Setup in DETI

Figure 5.3: Measurement Setup

5.3 Simple elliptical integrated lens antenna

As was done in the simulation an SEI lens was developed to test the manufacturing technique and measurement setup. This lens was made of PLA and has the dimensions described in table 5.1

The SEI lens antenna is used to improve the directivity of the source antenna, as concluded by simulation. Figures 5.4 and 5.5 and table 5.2 shows that this is precisely what happens; the HPBW decreases, using the SEI lens. The reflection coefficient has the expected behavior of varying the resonance frequency, with the presence of the lens.

Table 5.1: SEI lens antenna parameters

SEI lens antenna	
Lens dielectric constant	$\varepsilon_r = 2.63$
Small radius	$a = 40mm$
Large radius	$b = 43.24$
Distance from the lens center to the source antenna	$L = 16.44$
Patch antenna	
Total area	$44mm \times 44mm$
Patch dimensions	$10.63mm \times 10.63mm$

Table 5.2: HPBW for the SEI lens antenna with LP square patch antenna

Lens		**HPBW**			
		$\phi = 0°$		$\phi = 90°$	
		Without	**With**	**Without**	**With**
SEI lens antenna	**Simulation**	81°	34°	79°	29°
	Measurement	80°	27°	77°	35°

5.3.1 Results for the simple elliptical integrated lens antenna

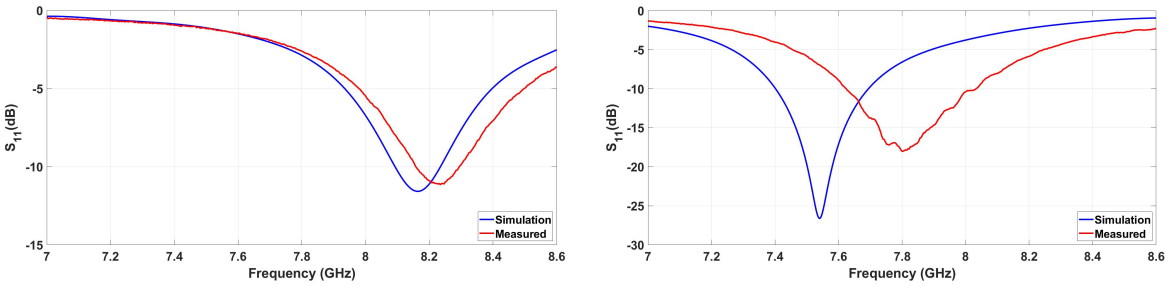

(a) Reflection coefficient without lens antenna **(b)** Reflection coefficient with lens antenna

Figure 5.4: Characteristics of the SEI lens antenna

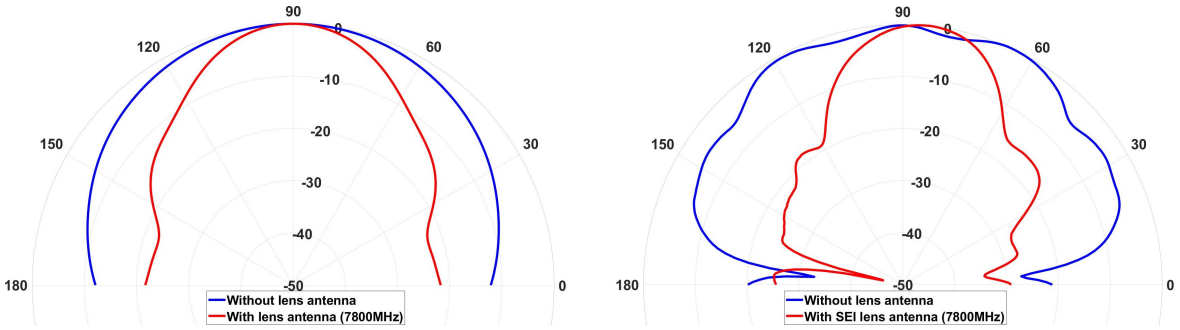

(a) Simulation results for $\phi = 0°$ **(b)** Measurement results for $\phi = 0°$

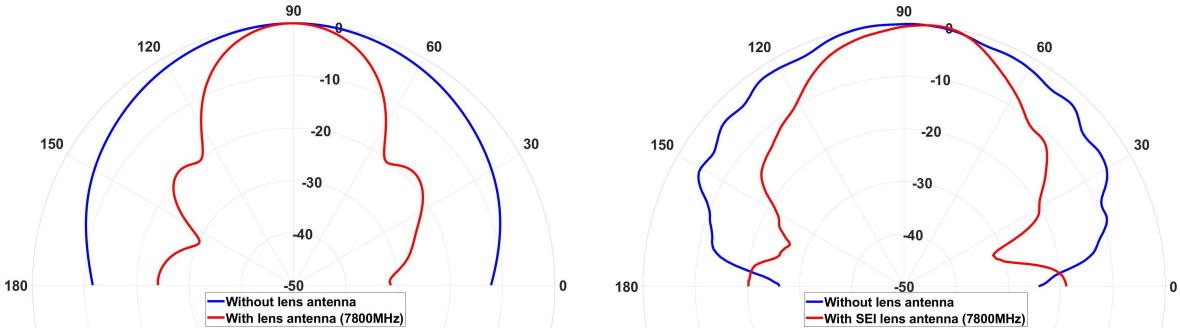

(c) Simulation results for $\phi = 90°$ **(d)** Measurement results for $\phi = 90°$

Figure 5.5: Normalized radiation pattern of the SEI lens antenna

5.4 Modified Half Maxwell Fish-Eye lens with a linearly polarized patch antennas

5.4.1 Results for the single-material lens antennas

Both lenses are compared to sample simulation because their dimensions are equal, and the layers' dielectric constants are very similar, providing equal simulation results. Comparing the results obtained by simulation and the measurement of the Reflection coefficient (figures 5.7, 5.9, and 5.11) shows that the lens's presence significantly impacts the resonance frequency and impedance of the patch antenna causing the patch antenna resonance frequency to drop, as well as the impedance to vary significantly (both in simulation and measurement). In the simulations, the patch and lens antennas have a resonance frequency of 7.8 GHz, although there is a slight deviation in resonance frequency. These deviations are due to imperfections in the characterization of the materials used and in the manufacturing method.

Figures 5.8, 5.10, and 5.12 and table 5.3 show that the lens antenna caused deformations on the radiation pattern (compared to the system without a lens). However, this variation is minimal, and one does not have a large beamwidth as expected.

These differences are largely caused by the infill (as can be seen in the figure 5.6) sometimes the filling pattern is not regular, which can cause differences in signal propagation inside the lens, and the constant transition between air and material can have unexpected refraction and reflection effects. The simulator assumes that the layers are uniformly filled with a homogeneous material, i.e., it does not consider the fact that the layers have different infills,

hence there are many differences between the simulated and measured values.

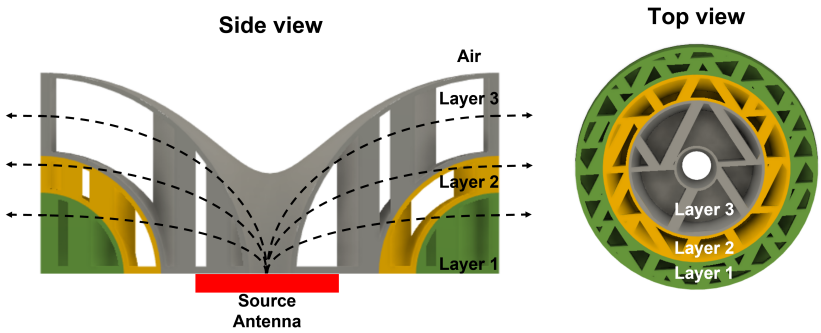

Figure 5.6: Example of the infill pattern of each layer (from top and profile view)

Table 5.3: HPBW for the single material MHMFE lens antennas

Lens		**HPBW**			
		$\phi = 0°$		$\phi = 90°$	
		Without	**With**	**Without**	**With**
3-Layers Single-material	**Simulation**	70°	142°	126°	136°
	CE3	72°	81°	117°	126°
	UM3E	72°	90°	117°	126°
4-Layers Single-material	**Simulation**	94°	158°	116°	136°
	CE3	81°	126°	117°	117°
	UM3E	81°	135°	117°	117°
5-Layers Single-material	**Simulation**	84°	154°	110°	153°
	CE3	72°	117°	126°	126°
	UM3E	72°	99°	126°	117°

Table 5.4: 3-Layers single material lens antenna parameters

3-Layer single material lens			
n-layer	1	2	3
Dielectric constant	2.26	2.01	1.00
Layer radius (mm)	10	19.7	22
Lens diameter	44mm		
Patch antenna			
Total area	$88mm \times 88mm$		
Patch dimensions	$10.715mm \times 10.715mm$		

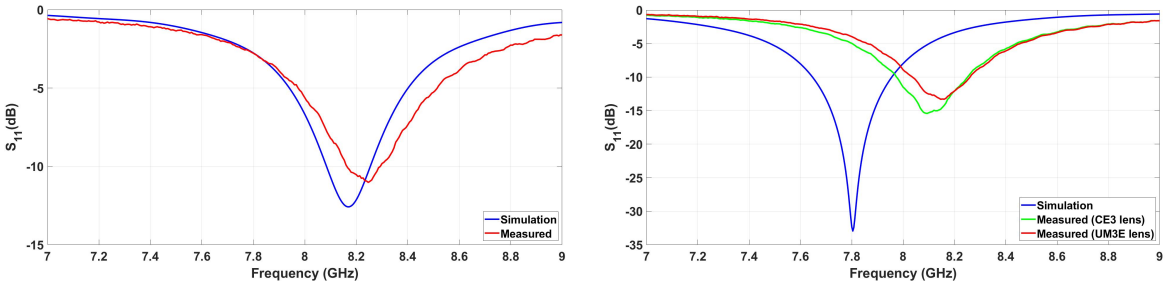

(a) Reflection coefficient without lens antenna **(b)** Reflection coefficient with lens antenna

Figure 5.7: Characteristics of the single material 3-layer lens antenna

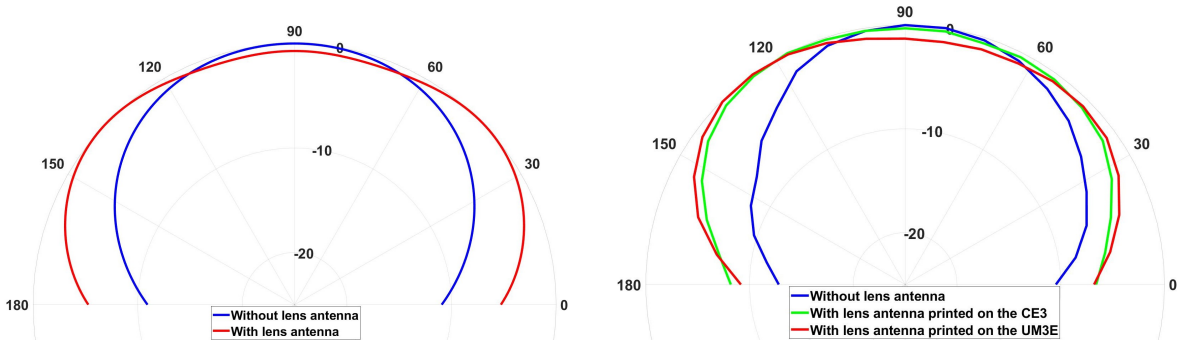

(a) Simulation results for $\phi = 0°$ **(b)** Measurement results for $\phi = 0°$

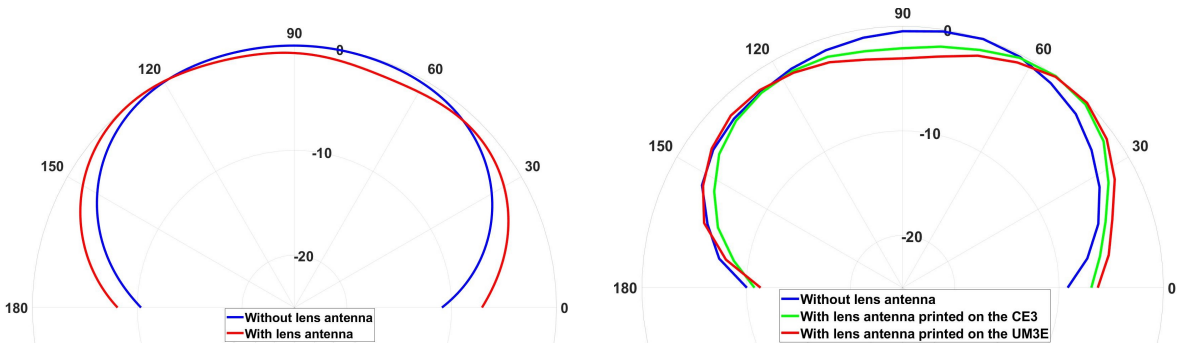

(c) Simulation results for $\phi = 90°$ **(d)** Measurement results for $\phi = 90°$

Figure 5.8: Normalized radiation pattern of the single material 3-layer lens antenna

Single material 4-layer lens antenna

Table 5.5: 4-Layers single material lens antenna parameters

4-Layer single material lens				
n-layer	1	2	3	4
Dielectric constant	2.25	2.15	2.01	1.00
Layer radius (mm)	9	13	22	25
Lens diameter	50mm			
Patch antenna				
Total area	$50mm \times 50mm$			
Patch dimensions	$10.705mm \times 10.705mm$			

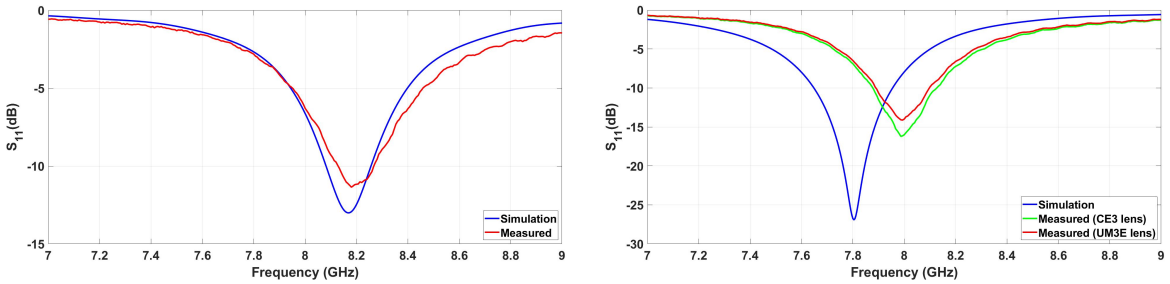

(a) Reflection coefficient without lens antenna **(b)** Reflection coefficient with lens antenna

Figure 5.9: Characteristics of the single material 4-layer lens antenna

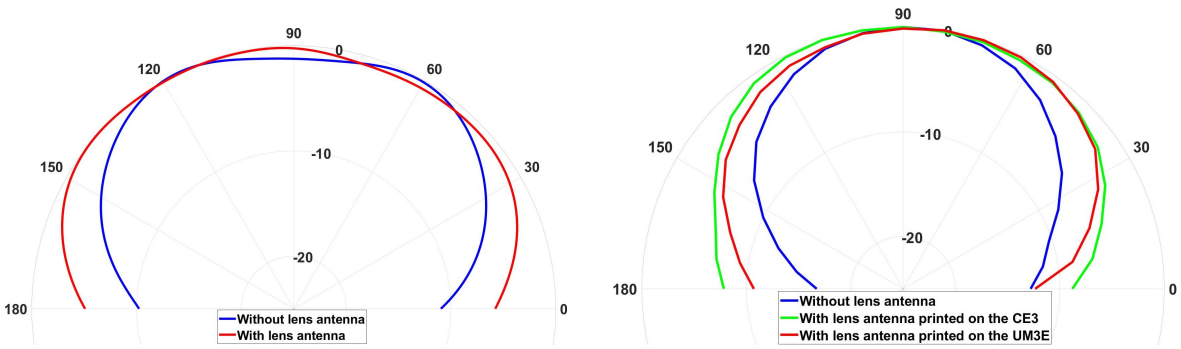

(a) Simulation results for $\phi = 0°$ **(b)** Measurement results for $\phi = 0°$

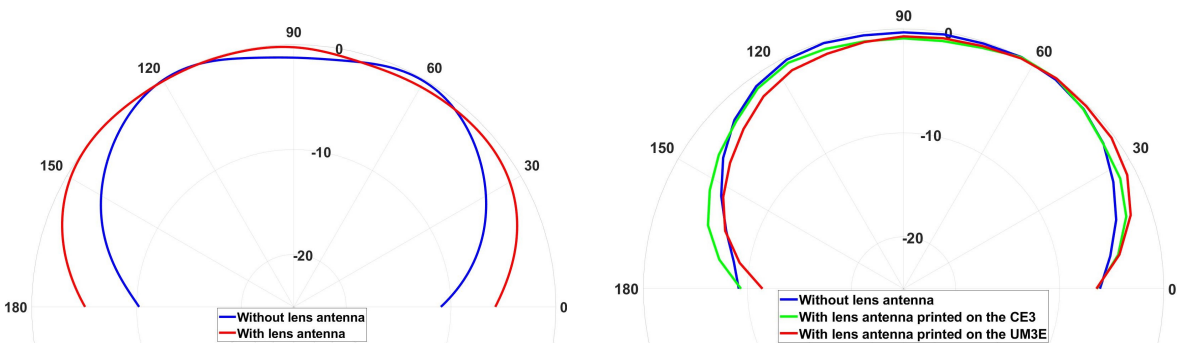

(c) Simulation results for $\phi = 90°$ **(d)** Measurement results for $\phi = 90°$

Figure 5.10: Normalized radiation pattern of the single material 4-layer lens antenna

Table 5.6: 5-Layers single material lens antenna parameters

5-Layer single material lens					
n-layer	1	2	3	4	5
Dielectric constant	2.27	2.15	2.06	2.01	1.00
Layer radius (mm)	4	8	12	22	25
Lens diameter	50mm				
Patch antenna					
Total area	$80mm \times 80mm$				
Patch dimensions	$10.63mm \times 10.63mm$				

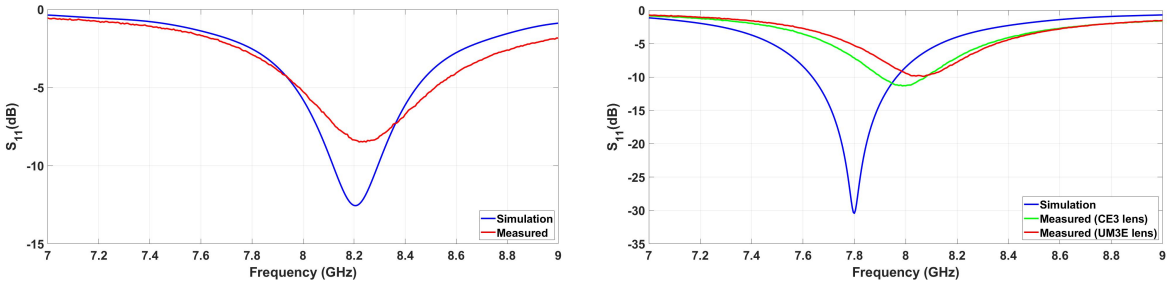

(a) Reflection coefficient without lens antenna **(b)** Reflection coefficient with lens antenna

Figure 5.11: Characteristics of the single material 5-layer lens antenna

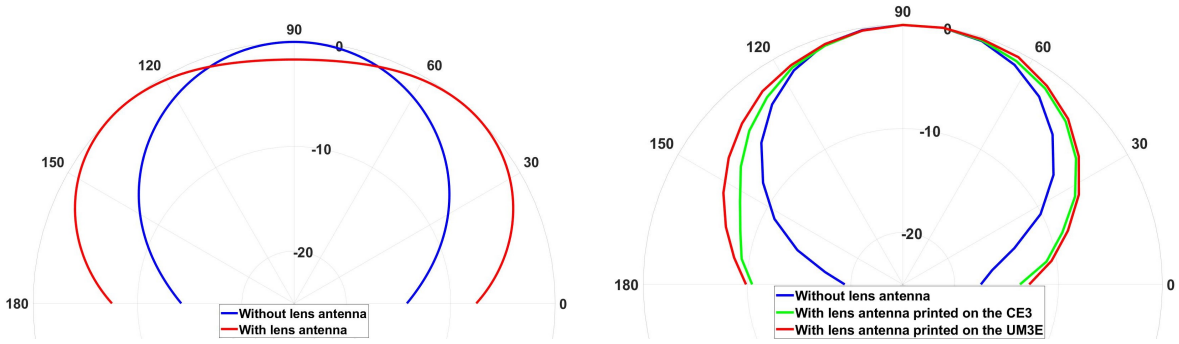

(a) Simulation results for $\phi = 0°$ **(b)** Measurement results for $\phi = 0°$

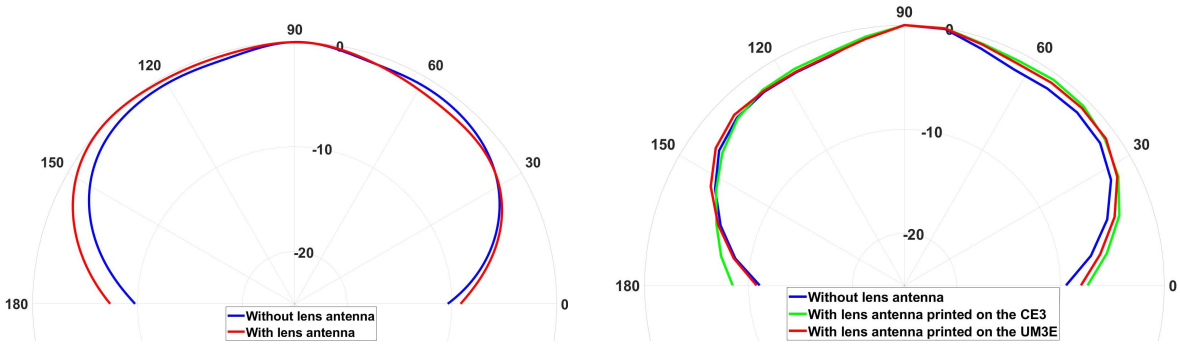

(c) Simulation results for $\phi = 90°$ **(d)** Measurement results for $\phi = 90°$

Figure 5.12: Normalized radiation pattern of the single material 5-layer lens antenna

5.4.2 Results for the multi-material lens antennas

The lens antennas with multiple materials are more complex than the lens antennas of a single material due to the use of multiple materials with different physical and printing characteristics. Therefore, as the UM3E printer allows the manufacture of two different materials simultaneously, the 3-layer lens antenna was manufactured in one piece (one extruder with Nylon and another with PETG). However, the 4-layer lens antenna requires a different approach using two different manufacturing methods:

- **Version 1** – Manufacture the layers individually and glue them together in one piece (with an adhesive layer added between layers).
- **Version 2** – Manufacture the most peripheral layers (PLA and PETG) and manufacture the missing layer (Nylon) separately. The two parts are press-fit together.

The radiation pattern (figures 5.14 and 5.16 and table 5.7) has the anticipated beamwidth increasing phenomenon. It is possible to observe for the $\phi = 0°$ (figures 5.14b and 5.16b)) that the radiation pattern significantly increases its beam aperture compared to the case of patch antenna without lens (as observed in the simulation). However, for the $\phi = 90°$ (figures 5.14d and 5.16d), the same does not happen. Several tests were made to verify this discrepancy of results, concluding that it was caused by the lens antenna. Therefore, another approach to achieve the desired results will have to be taken. The significant difference from the original article is the polarization of the source antenna, so the patch antennas were redesigned to have a circular polarization. So two patch antennas were created: a CP square patch antenna and a CP circular patch antenna (section 2.6.3).

Table 5.7: HPBW for the multi-material MHMFE lens antennas

Lens		**HPBW**			
		$\phi = 0°$		$\phi = 90°$	
		Without	**With**	**Without**	**With**
3-Layers Multi-material	**Simulation**	100°	158°	119°	140°
	Measurement	81°	135°	117°	54°
4-Layers Multi-material	**Simulation**	78°	146°	122°	134°
	Version 1	72°	145°	117°	27°
	Version 2	72°	154°	117°	36°

Table 5.8: 3-Layers multi-material lens antenna parameters

3-Layer single material lens			
n-layer	1	2	3
Dielectric constant	3.3380	2.7085	1
Layer radius (mm)	12	17.9	21
Lens diameter	42mm		
Patch antenna			
Total area	$54mm \times 54mm$		
Patch dimensions	$10.69mm \times 10.69mm$		

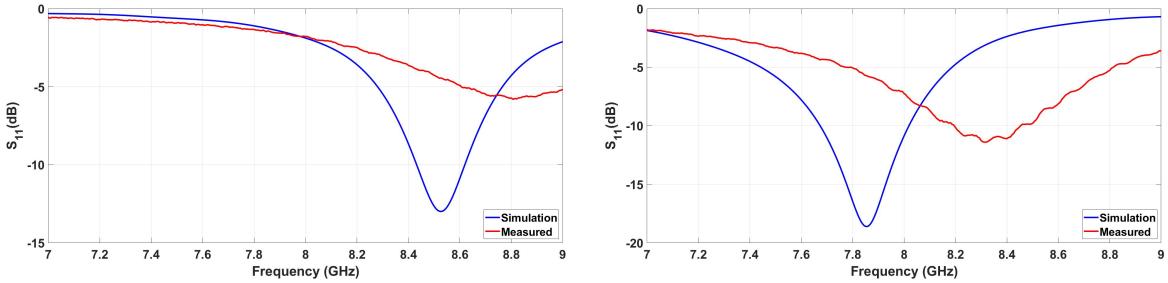

(a) Reflection coefficient without lens antenna **(b)** Reflection coefficient with lens antenna

Figure 5.13: Characteristics of the multi-material 3-layer lens antenna

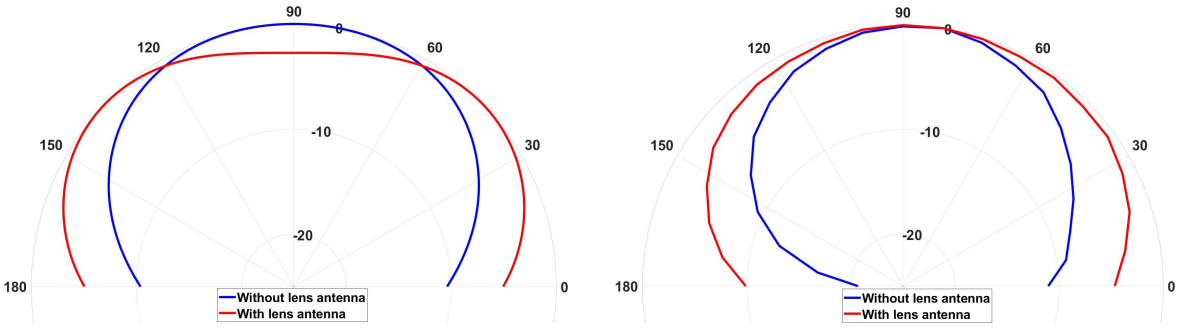

(a) Simulation results for $\phi = 0°$ **(b)** Measurement results for $\phi = 0°$

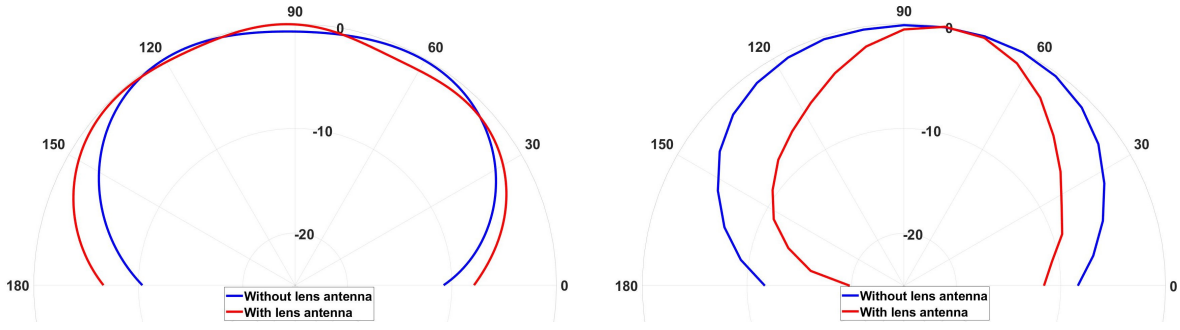

(c) Simulation results for $\phi = 90°$ **(d)** Measurement results for $\phi = 90°$

Figure 5.14: Normalized radiation pattern of the multi-material 3-layer lens antenna

Table 5.9: 4-Layers multi-material lens antenna parameters

4-Layer multi-material lens				
n-layer	1	2	3	4
Dielectric constant	3.34	2.71	2.63	1
Layer radius (mm)	5	10	19	21.75
Lens diameter	43.5mm			
Patch antenna				
Total area	$84mm \times 84mm$			
Patch dimensions	$10.6mm \times 10.6mm$			

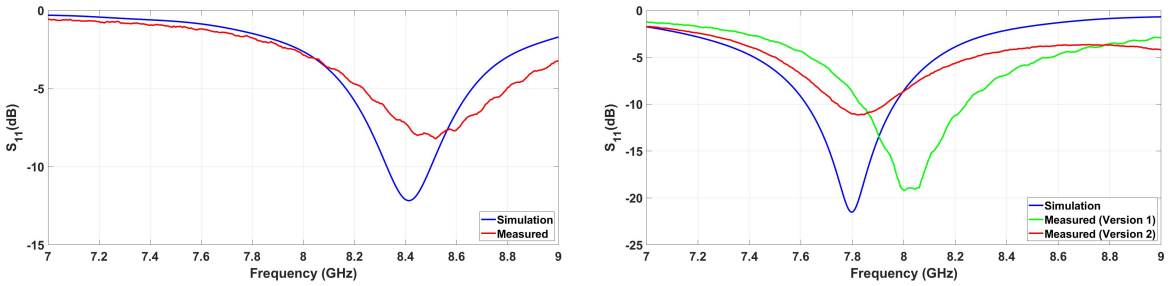

(a) Reflection coefficient without lens antenna **(b)** Reflection coefficient with lens antenna

Figure 5.15: Characteristics of the multi-material 4-layer lens antenna

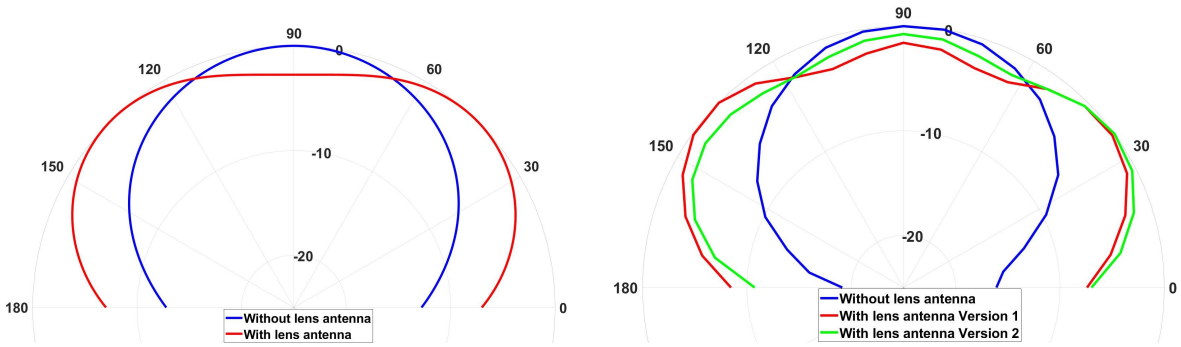

(a) Simulation results for $\phi = 0°$ **(b)** Measurement results for $\phi = 0°$

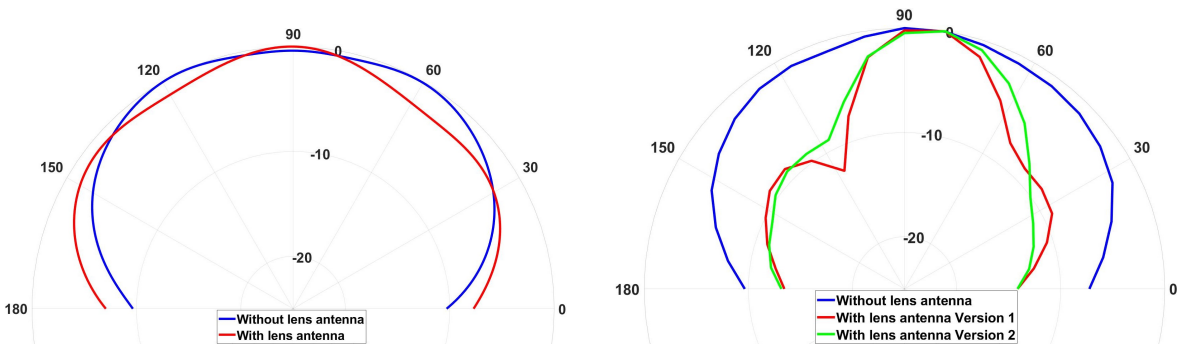

(c) Simulation results for $\phi = 90°$ **(d)** Measurement results for $\phi = 90°$

Figure 5.16: Normalized radiation pattern of the multi-material 4-layer lens antenna

5.5 Modified Half Maxwell Fish-Eye lens with a circular polarized patch antennas

This test sequence puts under test the use of two circularly polarized patch antennas: a CP square patch and a CP circular patch (figure 5.17). Furthermore, both versions (glued and press-fitted) of the 4-layer multi-material lens antenna (equal to the one used on previous tests). The objective of these tests is to determine if in fact the use of CP antennas is more beneficial than the use of LP antennas since similar articles have used polarization CP antennas [2].

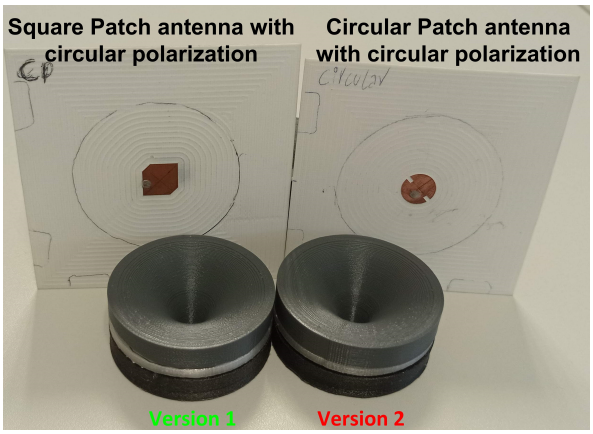

Figure 5.17: Patch antennas with CP manufactured

It was clear from the start that designing, in simulation, a lens and patch antenna with CP was a more time-consuming process due to the many variables that can be adjusted and the high simulation time. The physical measurements also have to be more precise. Any deviation in the antennas' alignment can lead to errors. For this reason, the DETI anechoic chamber was used.

5.5.1 Results for the square patch with circular polarization

From figures 5.18 to 5.20 and table 5.11, both the lens antennas have a similar performance and do not perform as expected. Although the antennas have a good performance in simulation, the results of the measurements show quite a few discrepancies.

Although the resonance frequency is a little higher, it is still within the expected boundaries. However, the same cannot be applied to the Axial Ratio, which has a higher frequency but with a worse performance, which is very close to 3dB leading to a weak CP of the antenna. So, to increase the possibility of the lens antenna performing as required, the radiation patterns were measured at the frequency with the best axial ratio (8GHz for the lens antenna version 1 and 8.11GHz for the lens antenna version 2).

Nevertheless, none of the lens antennas significantly increases the aperture of the radiation beams compared to the case of the patch without lens antennas. As can be seen from figures 5.19 and 5.20, the measured radiation pattern of the patch without a lens antenna is relatively similar to the simulation. The radiation pattern of the patch with the lens antennas does not show any significant improvement, making the radiation pattern more irregular and reducing the beam aperture, thus being very different from what was expected by simulation.

Table 5.10: Square patch with circular polarization dimensions

CP square patch antenna	
Total area	$84mm \times 84mm$
Patch dimensions	$11mm \times 11mm$
Cut dimension (dim_{cut})	2.5mm

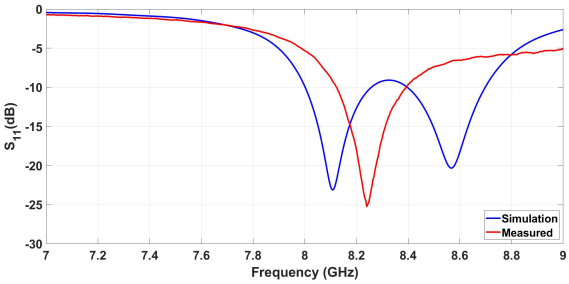

(a) Reflection coefficient without lens antenna

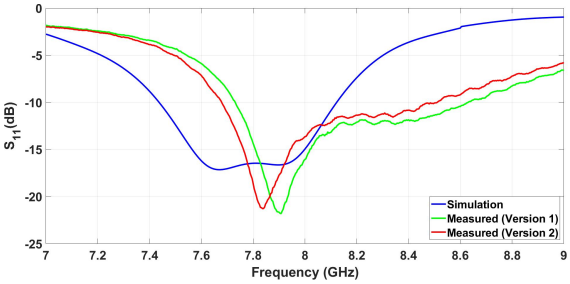

(b) Reflection coefficient with lens antenna

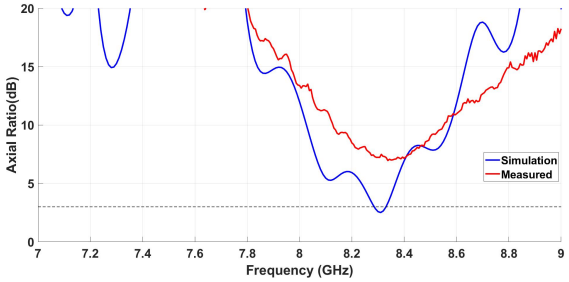

(c) Axial ratio without lens antenna

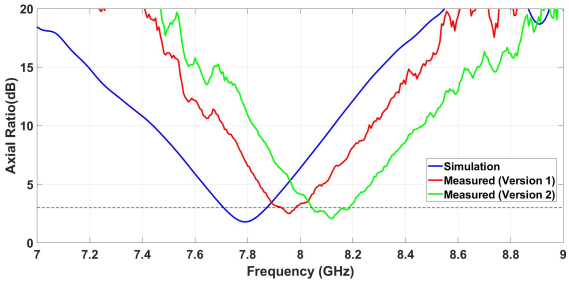

(d) Axial ratio with lens antenna

Figure 5.18: Characteristics of the multi-material 4-layer lens antenna with CP square patch antenna

Table 5.11: HPBW for the multi-material 4-layer lens antenna with CP square patch antenna

Lens		**HPBW**			
		$\phi = 0°$		$\phi = 90°$	
		Without	**With**	**Without**	**With**
4-Layers Multi-material	**Simulation (8GHz)**	74°	121°	120°	141°
	Version 1 (8GHZ)	94°	33°	86°	66°
	Simulation (8.110GHz)	74°	85°	140°	140°
	Version 2 (8.110 GHz)	87°	25°	81°	50°

MHMFE lens antenna version 1 + square patch antenna with CP

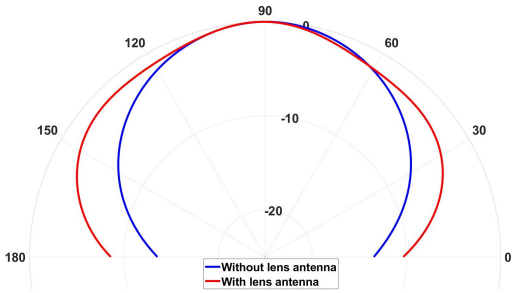

(a) Simulation results for $\phi = 0°$

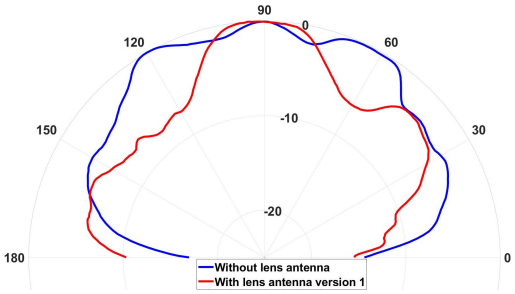

(b) Measurement results for $\phi = 0°$

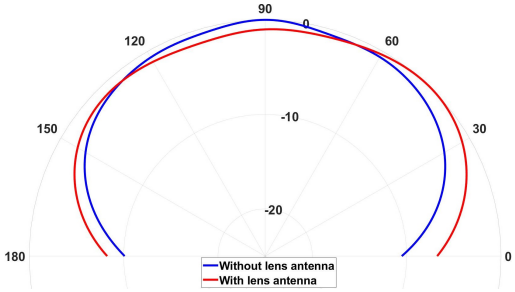

(c) Simulation results for $\phi = 90°$

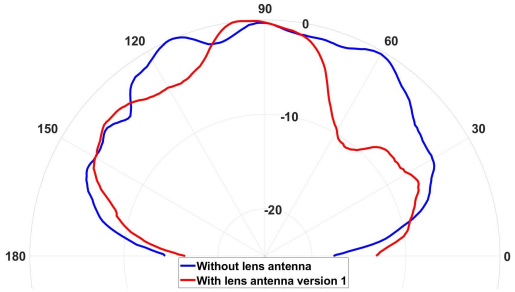

(d) Measurement results for $\phi = 90°$

Figure 5.19: Normalized radiation pattern of the version 1 lens antenna with CP square patch antenna (8GHz)

MHMFE lens antenna version 2 + square patch antenna with CP

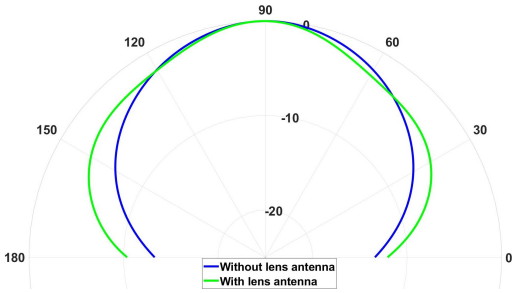

(a) Simulation results for $\phi = 0°$

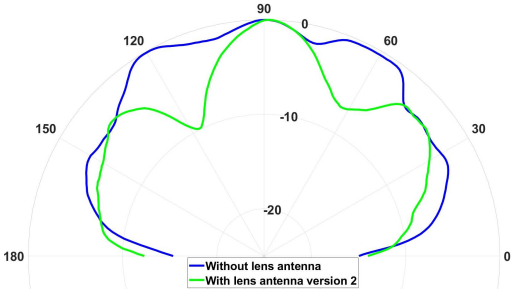

(b) Measurement results for $\phi = 0°$

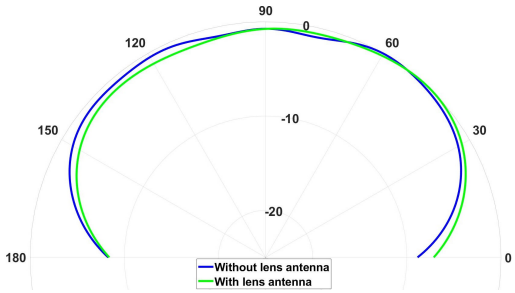

(c) Simulation results for $\phi = 90°$

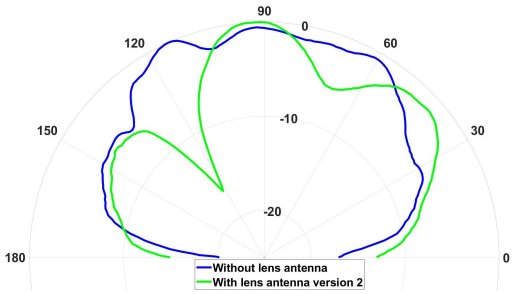

(d) Measurement results for $\phi = 90°$

Figure 5.20: Normalized radiation pattern of the version 2 lens antenna with CP square patch antenna (8.11GHz)

5.5.2 Results for the circular patch with circular polarization

The circular patch with circular polarization had a very different behavior from the simulations. For this reason, it was considered that this antenna was not properly designed, and the results obtained were discarded.

CHAPTER 6

Conclusions and Future Work

This chapter presents the conclusions of the work developed and suggestions for future work.

6.1 Conclusions

After testing several antennas by simulation, it was concluded that SEI the lens antenna performs very similarly to the simulated one and the MHMFE structure could manipulate the radiation pattern, more specifically increase the HPBW by about 80%. Furthermore, it was possible to study the impact on the resonance frequency and impedance of the source antenna.

The prototype SEI lens antenna has the desired behavior, similar to that observed in the simulation of the same lens, being able to reduce the HPBW by about 40%, making the antenna very directive. However, some deformations can be observed in the radiation pattern when compared to the simulation. These variations are caused mainly by the fabrication of the lens, which is not perfect even though the antenna is very simple to fabricate.

The more challenging task, for the MHMFE lenses, was to replicate the simulations with a real antenna. Several prototypes were manufactured using different materials, sizes, and layers and tested using patch antennas with various dimensions and polarizations. The best results were obtained for a multi-material lens and a LP patch antenna, the HPBW increased significantly for $\phi = 0°$ but not for $\phi = 90°$. The single-material MHMFE and a LP patch antenna also provide a uniform radiation pattern, and slightly increase the HPBW. Using CP patch antennas as a source proved to be a highly complex design to simulate and measure, And the results are not reliable enough to draw any accurate conclusions, requiring further analysis.

The manufacturing method, 3D printing, causes the differences between the simulations and the prototypes antennas. The simulator considers the lens body as having uniform layers of material with a clean transition between layers. On the other hand, the 3D printed lens does not have uniform material (due to material contaminations or other manufacturing defects),

and sometimes the parts require some hand-fitting (such as sanding or gluing) that may lead to minor alterations to the structure. Thus, it would be interesting to use a simulator that considers these to obtain more realistic results.

The SMLC method provided a reasonable and easy characterization, although it only was possible to characterize three materials (PLA, PETG, and Nylon), limiting the maximum number of layers that the MHMFE lens can have. The characterization of more materials leads to antennas with more layers of different materials, leading to better results. Another option is to use a different manufacturing method that allows using different materials and a more precise lens manufacturing.

Concluding, the MHMFE lens antenna has the potential to increase the HPBW over 160° in both planes. However, the combination of several effects (such as few layers, material characterization inaccuracies, manufacturing imperfections, and measurement problems) may have led to underperforming results. Still, this research collected some essential information that can be a foundation for future work.

6.2 Future Work

The study done in this dissertation opened several possibilities for the design and manufacture of new MHMFE lens antennas. The next major step will be to characterize more dielectric materials, such as plastic polymers with different characteristics or other unusual materials compatible with 3D printing, allowing to manufacture of lens antennas with more layers and different dielectric constant values.

3D printing (FDM) was the chosen technology, because allows for the fastest and easiest prototyping. However, there are many more manufacturing methods compatible with the manufacture of lens antennas. A possible future work would be to study and experiment with new fabrication techniques for lens antennas, which can mitigate some of the problems caused by 3D printing.

The simulator used is not an accurate representation of reality because, as previously mentioned, the simulator does not consider some aspects of the real prototype, such as infilling the layers. It would be interesting to study a way to obtain simulations closer to the actual system, either by more accurate manufacture of the antennas or by improving the simulations or using another more realistic simulator. Also, using other types of source antennas would be interesting future work, potentially using this type of lens in other applications.

Nevertheless, the most crucial future work would be to study the application of MHMFE lens antennas in phased arrays to increase the beamwidth.

Bibliography

[1] C. Fernandes and E. Lima, "Dielectric lens antennas," in Sep. 2016, pp. 1001–1064, ISBN: 978-981-4560-43-6. DOI: 10.1007/978-981-4560-44-3_40.

[2] Z. Yi and Q. Zhu, "A novel half maxwell fish-eye lens for wide beamwidth antennas," *2016 IEEE Antennas and Propagation Society International Symposium, APSURSI 2016 - Proceedings*, vol. 3, pp. 1927–1928, 2016.

[3] D. Helena, A. Ramos, T. Varum, and J. N. Matos, "Antenna design using modern additive manufacturing technology: A review," *IEEE Access*, vol. 8, pp. 177 064–177 083, 2020. DOI: 10.1109/ACCESS.2020.3027383.

[4] D. Bodnal, "Lens Antennas," in *Antenna Engineering Handbook*, R. Johnson, Ed., 3rd ed., Atlanta, Georgia: McGraw-Hill, Inc., 1993, ch. 16, pp. 534–565.

[5] A. Boriskin, R. Sauleau, and C. Fernandes, "Integrated lens antennas," in Jan. 2018, pp. 3–36, ISBN: 978-3-319-62772-4. DOI: 10.1007/978-3-319-62773-1_1.

[6] Z. Sipus and T. Komljenovic, "Multi-shell radially symmetrical lens antennas," in Jan. 2018, pp. 37–73, ISBN: 978-3-319-62772-4. DOI: 10.1007/978-3-319-62773-1_2.

[7] D. F. Filipovic, G. M. Rebeiz, and S. S. Gearhart, "Double-slot antennas on extended hemispherical and elliptical quartz dielectric lenses," *International Journal of Infrared and Millimeter Waves*, vol. 14, pp. 1905–1924, 1993. DOI: 10.1007/BF02096363.

[8] Z. L. Mei, J. Bai, T. M. Niu, and T. J. Cui, "A half maxwell fish-eye lens antenna based on gradient-index metamaterials," *IEEE Transactions on Antennas and Propagation*, vol. 60, no. 1, pp. 398–401, 2012. DOI: 10.1109/TAP.2011.2167914.

[9] B. Fuchs, O. Lafond, S. Rondineau, and M. Himdi, "Design and characterization of half maxwell fish-eye lens antennas in mm-waves," *Microwave Theory and Techniques, IEEE Transactions on*, vol. 54, pp. 2292–2300, Jul. 2006. DOI: 10.1109/TMTT.2006.875255.

[10] *Guide to Manufacturing Processes for Plastics*. [Online]. Available: https://formlabs.com/blog/guide-to-manufacturing-processes-for-plastics/#injection-molding (visited on 06/24/2021).

[11] The British Standards Institution ISO/ASTM, "ISO/ASTM 52900: Additive manufacturing - General principles and Terminology," *International Standard*, vol. 5, no. 978-84-9042-335-6, pp. 1–26, 2015. [Online]. Available: https://www.iso.org/obp/ui/#iso:std:69669:en%0Ahttps://www.iso.org/standard/69669.html%0Ahttps://www.astm.org/Standards/ISOASTM52900.htm.

[12] B. Redwood, F. Schffer, and B. Garret, *The 3D Printing Handbook: Technologies, Design and Applications*, 1st. 2017, ISBN: 9082748509.

[13] *Which Layer Height is Best for 3D Printing? - 3D Printerly*. [Online]. Available: https://3dprinterly.com/which-layer-height-is-best-for-3d-printing/ (visited on 06/24/2021).

[14] *How to Get the Perfect Shell Thickness Setting - 3D Printing - 3D Printerly*. [Online]. Available: https://3dprinterly.com/how-to-get-the-perfect-shell-thickness-setting-3d-printing/ (visited on 06/24/2021).

[15] *The importance of the type of infill in 3D printing*. [Online]. Available: https://filament2print.com/gb/blog/71_importance-infill-3d-printing.html (visited on 06/24/2021).

[16] *Selecting the optimal shell and infill parameters for FDM 3D printing | Hubs*. [Online]. Available: https://www.hubs.com/knowledge-base/selecting-optimal-shell-and-infill-parameters-fdm-3d-printing/ (visited on 06/24/2021).

[17] Z. Raheem, "Physics of dielectrics," in May 2010, pp. 3–16, ISBN: 9780750662680. DOI: 10.1016/B978-075066268-0/50003-2.

[18] P. Veselý, T. Tichý, O. Sefl, and E. Horynová, "Evaluation of dielectric properties of 3d printed objects based on printing resolution," *IOP Conference Series: Materials Science and Engineering*, vol. 461, p. 012 091, Dec. 2018. DOI: 10.1088/1757-899X/461/1/012091.

[19] E. Huber, M. Mirzaee, J. Bjorgaard, M. Hoyack, S. Noghanian, and I. Chang, "Dielectric property measurement of pla," May 2016, pp. 0788–0792. DOI: 10.1109/EIT.2016.7535340.

[20] A. Goulas, S. Zhang, D. Cadman, *et al.*, "The impact of 3d printing process parameters on the dielectric properties of high permittivity composites," *Designs*, vol. 4, Nov. 2019. DOI: 10.3390/designs3040050.

[21] S. Zhang, C. Njoku, W. Whittow, and J. Vardaxoglou, "Novel 3d printed synthetic dielectric substrates," *Microwave and Optical Technology Letters*, vol. 57, pp. 2344–2346, Jul. 2015. DOI: 10.1002/mop.29324.

[22] H. Hu, S. Sinha, N. Meisel, and S. Bilén, "Permittivity of 3d-printed nylon substrates with different infill patterns and densities for design of microwave components," *Designs*, vol. 4, Sep. 2020. DOI: 10.3390/designs4030039.

[23] J. C. Booth, M. Whitley, C. Rudd, and M. Kranz, "Material database for additive manufacturing techniques," *Technical Report RDMR-WD-17-64*, no. December, 2017. [Online]. Available: https://apps.dtic.mil/sti/pdfs/AD1043719.pdf.

[24] Ultimaker, "Technical data sheet: Nylon," pp. 1–3, 2017. [Online]. Available: https://fillamentum.com/collections/technical-polymers/products/nylon-cf15-carbon.

[25] T. B. Group, "Technical data sheet PETG," vol. 123, pp. 98–99, 2013.

[26] Ultimaker, "Technical data sheet - Ultimaker PLA," pp. 1–3, 2018. [Online]. Available: https://ultimaker.com/download/74970/UM180821%20TDS%20PLA%20RB%20V11.pdf.

[27] J. Baker-Jarvis, R. Geyer, J. Jr, *et al.*, "Dielectric characterisation of low-loss materials—a comparison of techniques," *Dielectrics and Electrical Insulation, IEEE Transactions on*, vol. 5, pp. 571–577, Sep. 1998. DOI: 10.1109/94.708274.

[28] C.-K. Lee, J. McGhee, C. Tsipogiannis, *et al.*, "Evaluation of microwave characterization methods for additively manufactured materials," *Designs*, vol. 3, p. 47, Sep. 2019. DOI: 10.3390/designs3040047.

[29] R. Gonçalves, "Antenna design for passive sensors in non-conventional materials," Doutoramento em Engenharia Eletrotécnica, Universidade de Aveiro, 2016, p. 270.

[30] C. A. Balanis, *Antenna Theory: Analysis and Design*. USA: Wiley-Interscience, 2017, ISBN: 978-1-118-64206-1.

[31] S. Mat Salleh, M. Jusoh, A. Ismail, N. Yasin, M. Kamarudin, and R. Yahya, "Circular polarization textile antenna for gps application," *Lecture Notes in Electrical Engineering*, pp. 255–263, Jan. 2014. DOI: 10.1007/978-3-319-17269-9_28.

[32] T. Varum, J. Matos, and P. Pinho, "Non-uniform microstrip antenna array for dsrc in single-lane structures," *Sensors (Basel, Switzerland)*, vol. 16, Dec. 2016. DOI: 10.3390/s16122101.

[33] Simulia, *Cst studio suite 3d em simulation and analysis software*, [Online; Acedido a 30 de Março de 2021]. [Online]. Available: https://www.3ds.com/products-services/simulia/products/cst-studio-suite/.

[34] E. Lima, M. Silveirinha, C. Fernandes, and J. Costa, "Ilash - software tool for the design of integrated lens antennas," Aug. 2008, pp. 1–4. DOI: 10.1109/APS.2008.4619133.

[35] R. Corporation, "RO4725JXR & RO4730G3 Data Sheet," Tech. Rep., 2021, p. 4.

[36] Keysight, *MATLAB - LAN as Socket- Binary Block File Transfer*. [Online]. Available: http://na.support.keysight.com/fieldfox/help/Programming/webhelp/Examples/MATLAB/MATLAB_-_Sockets-_Binary_Block_File_Transfer.htm (visited on 06/21/2021).

Appendix A

Characterization process of the Single Microstrip Line Characterization method

This method only requires a sample of the material with a conductive line and ground plane, a VNA, and some mathematical calculations. Therefore, to do the characterization of the dielectric constant of the material, the following steps are followed:

1. A material sample of known dimensions (length L, width W_s and height h) with a line of conductive material (such as copper tape) of width W_l is manufactured to be put under test (figure 1).
2. Measure the input impedance ($Z_{in} = R - jX$) at a quarter of the first resonance frequency ($\frac{f_r}{4}$)
3. With this value, the value of αl is discovered using the following equation:

$$\alpha l = arctanh(-\frac{X}{R} + \sqrt{(\frac{X}{R})^2 + 19} \tag{6.1}$$

4. This value will allow calculating the correct resonance frequency $f_r' = \frac{f_r}{(1+\alpha l)}$
5. The input impedance is measured again ($Z_{in}' = R' - jX'$) but for a quarter of the correct resonance frequency ($\frac{f_r'}{4}$)
6. Recalculate the value of $\alpha l'$ (from the equation 6.1) and calculate the characteristic impedance for the correct resonant frequency

$$Z_0' = X' \times \frac{1 + (\tanh(\alpha l'))^2}{1 - (\tanh(\alpha l'))^2} = R' \times \frac{1 + (\tanh(\alpha l'))^2}{2 \times \tanh(\alpha l')} \tag{6.2}$$

7. Calculate the effective dielectric constant of the material (ε_{reff}):

$$\begin{aligned} \varepsilon_{reff} &= (\frac{60}{Z_0'} \times \ln(\frac{8h}{W_l} + \frac{W_l}{4h}))^2\,,\ para\ \frac{W_l}{h} \leq 1 \\ \varepsilon_{reff} &= (\frac{120\pi}{Z_0'} \times \frac{1}{\frac{W_l}{h} + 1,393 + 0,667 \times \ln(\frac{W_l}{h} + 1,444)})^2\,,\ para\ \frac{W_l}{h} > 1 \end{aligned} \tag{6.3}$$

8. Finally, calculate the dielectric constant of the material(ε_r):

$$\varepsilon_r = \frac{2 \times \varepsilon_{reff} + \frac{1}{\sqrt{1+\frac{12h}{W_l}}} - 1}{1 + \frac{1}{\sqrt{1+\frac{12h}{W_l}}}} \tag{6.4}$$

The characterization of the tangent of losses ($\tan(\delta)$) of the material is also done with an iterative method, which starts from the characteristic impedance (Z_0') calculated in the dielectric constant and applies several calculations until an approximate value of the tangent of losses is reached. Therefore, the value of the tangent of losses can be obtained through the following steps:

1. The first approximation of the loss tangent ($\tan(\delta)$)) is calculated from the characteristic impedance (Z_0') calculated on the dielectric constant:

$$\begin{aligned} \tan(\delta) &= \frac{0,0195 \times Z_0' - 0,274}{Z_{in}} \\ Z_{in} &= 1,95 \times Z_0' - 27,4 \end{aligned} \tag{6.5}$$

2. Calculate the value of K and τ (σ_a is the conductivity of the line)

$$\begin{aligned} K &= \frac{a_K}{\sqrt{\sigma_a}} + b_K \\ a_K &= 0,475 - 2,105 \times \tan(\delta) \\ b_K &= \frac{0,0644}{\sqrt{\tan(\delta)}} - 0,203 \end{aligned} \tag{6.6}$$

$$\begin{aligned} \tau &= \frac{a_\tau}{\sqrt{\sigma_a}} + b_\tau \\ a_\tau &= 115,6 - 1991,0 \times \tan(\delta) \\ b_\tau &= \frac{1,097}{\sqrt{\tan(\delta)}} + 95,53 \end{aligned} \tag{6.7}$$

3. The new input impedance (Z_m) is calculated (the line width value (W_l) must be in millimeters)

$$Z_m = Z_{in} \times (1 - K \times e^{\frac{Z_0' \times W_l}{\tau}}) \tag{6.8}$$

4. The input impedance is substituted to the new input impedance ($Z_{in} = Z_m$) and the loss tangent is recalculated using the equation 6.5
5. Repeat this step sequence at least four times to have a realistic approximation of the loss tangent

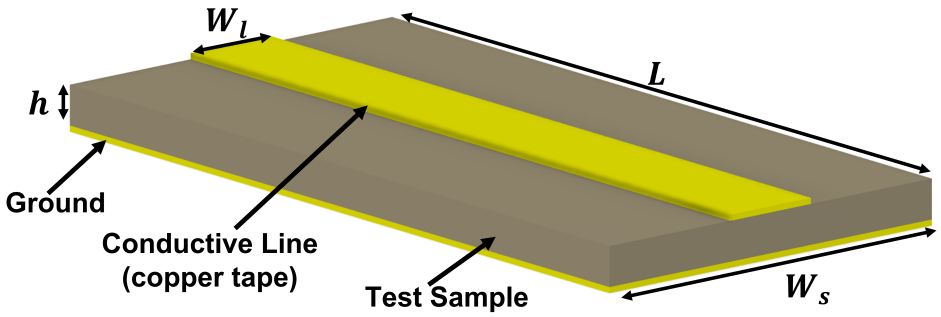

Figure 1: Test sample for the SMLC method

Appendix B

How to design an Simple Elliptical Integrated lens antenna

The first step is to draw a sphere of radius a and centered at $(x, y, z) = (0, 0, L)$ with a material with the desired dielectric constant and radius a (figure 2a). The transformation of a sphere into an ellipsoid requires an elongation along the z-axis to the desired size of the large radius (b) (figure 2b). The final step is to cut the ellipsoid, so all the lens material in the negative part of the z-axis is discarded (figures 2c and 2d).

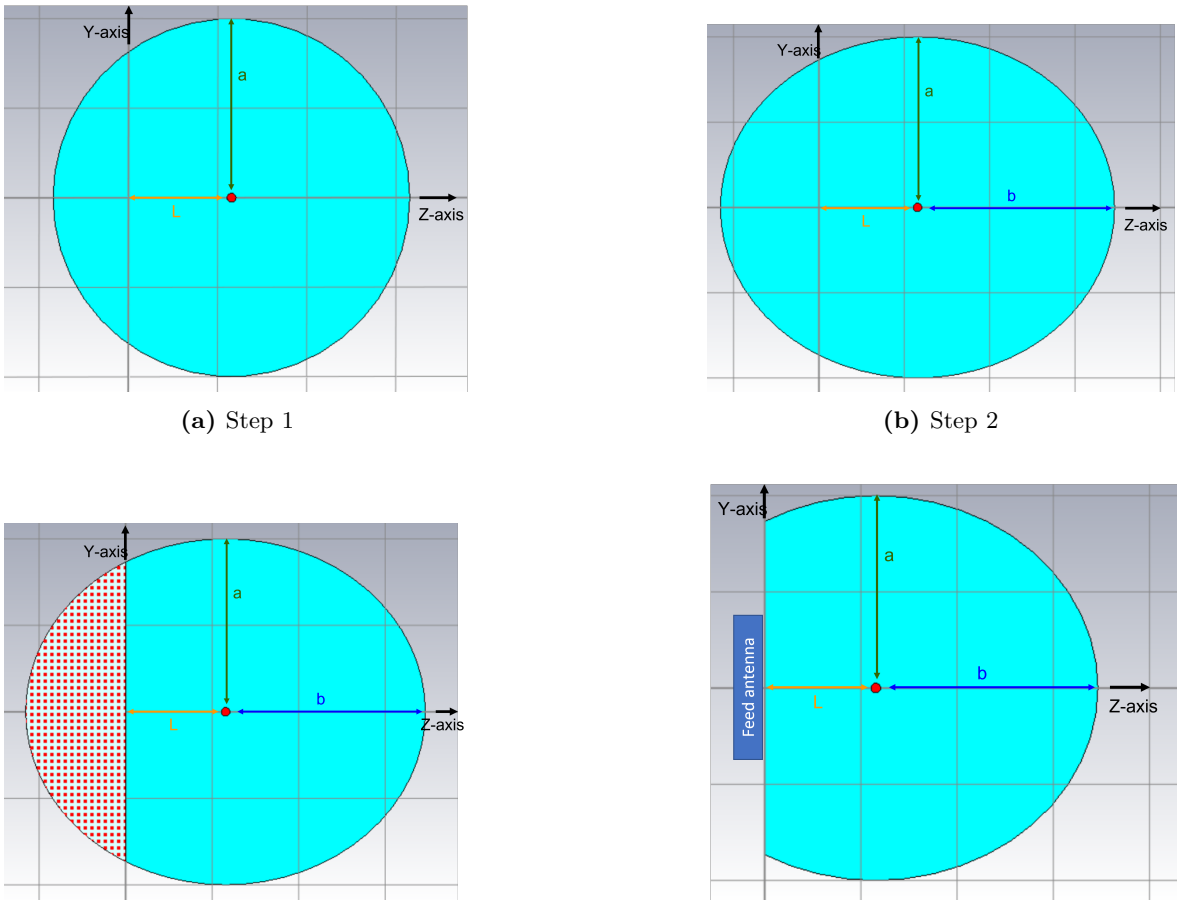

(a) Step 1

(b) Step 2

(c) Step 3

(d) Step 4

Figure 2: How to build an SEI lens antenna (2D View)

Appendix C

How to design an Modified Half Maxwell Fish-Eye lens antenna

Designing an MHMFE antenna lens in *CST Studio Suite* is an iterative process building one layer at a time, so each layer is designed as follows:

1. The first step is to draw a ring in the x-plane with an outer radius r_{10}, inner radius r_9, center at $(y, z) = (R, front)$ (where front is the distance from the base of the source antenna to its front the sum of copper height and substrate height for patch antenna). And a material with the dielectric constant of the respective layer. (figures 3a and 3b)
2. In the design of an MHMFE, only a quarter ring is needed, and two rectangles are drawn in the same plane as the ring. The first rectangle has the dimensions $(y_{min}, y_{max}) = (R, D)$ and $(z_{min}, z_{max}) = (-(R + front), R + front)$ and the second rectangle has the dimensions $(y_{min}, y_{max}) = (0, D)$ and $(z_{min}, z_{max}) = (-(R + front), R + front)$)=(-(R+front),front), as shown in figure 3c. The quarter ring is obtained by subtracting these rectangles from the ring (figure 3d).
3. The last step to obtain the layer is to rotate 360°° around the z-axis, as exemplified in figures 3e and 3f.
4. After this, repeat all the steps for the remaining layers.

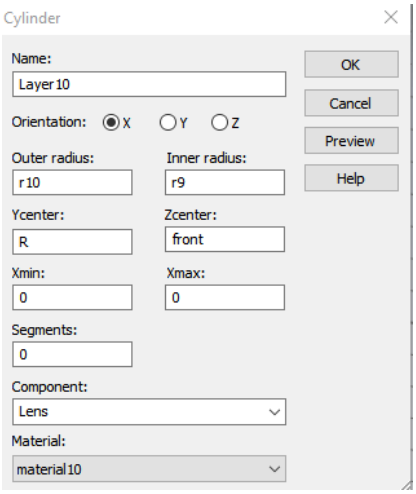

(a) Step 1

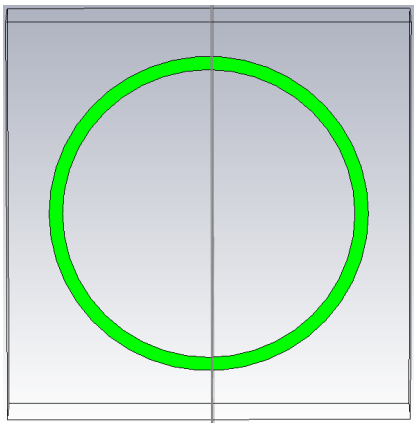

(b) Step 2

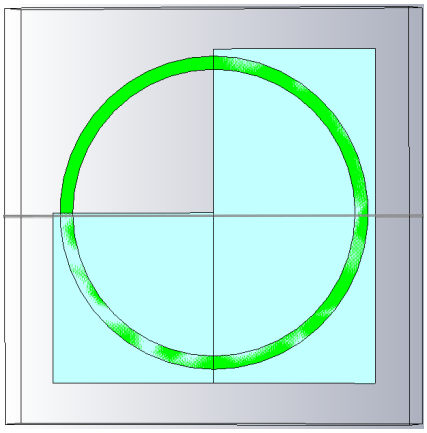

(c) Step 3

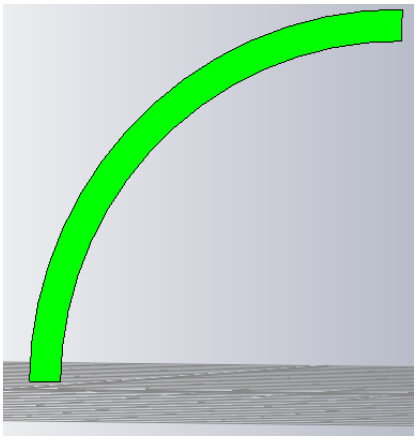

(d) Step 4

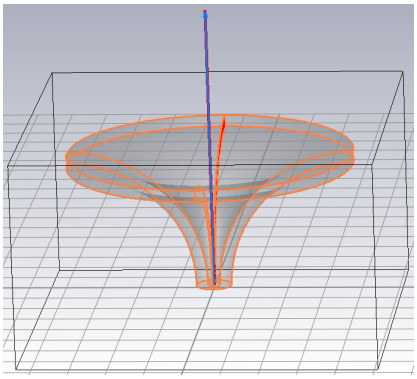

(e) Step 5

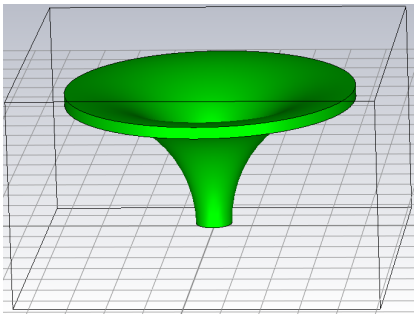

(f) Step 6

Figure 3: How to build an MHMFE lens antenna

Appendix D

Dielectric characterization of 3D printed materials

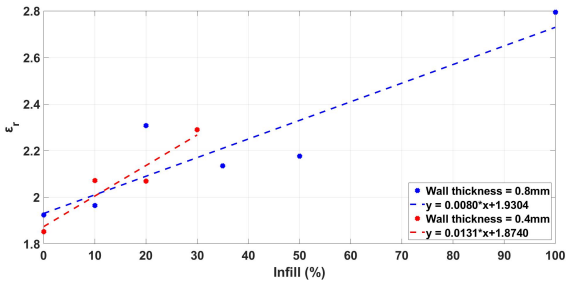

(a) Sample printed on the CE3

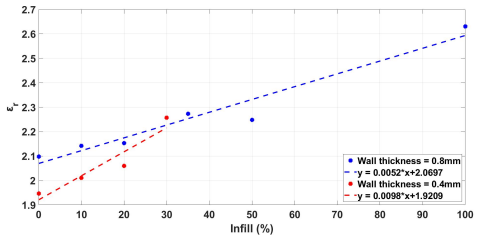

(b) Sample printed on the UM3E

Figure 4: Results of the Dielectric characterization of the PLA samples

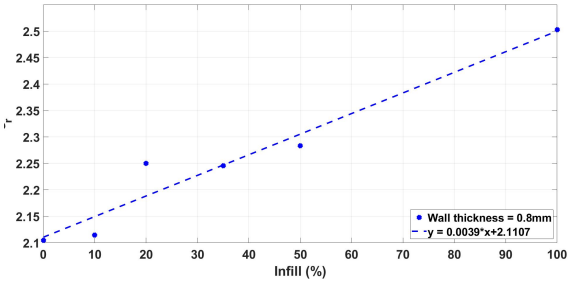

(a) Sample printed on the CE3

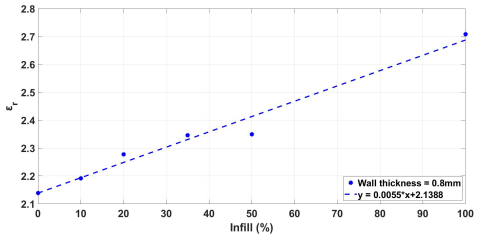

(b) Sample printed on the UM3E

Figure 5: Results of the Dielectric characterization of the PETG samples

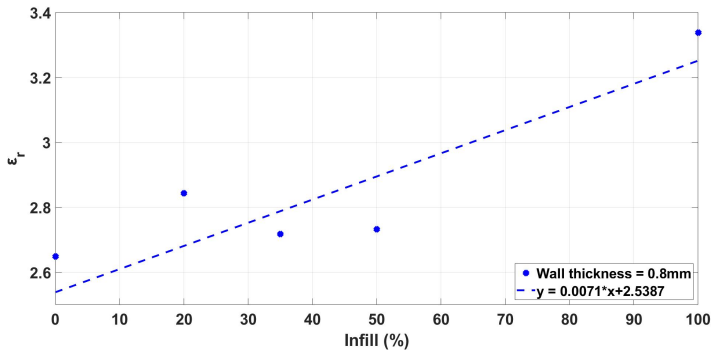

Figure 6: Results of the Dielectric characterization of the Nylon samples

Table 1: Characterisation of the 3D printed samples

Printer	Filament	Filament Brand	Height (mm)	Length (mm)	Width (mm)	Nozzle (mm)	Resolution (mm)	Base thickness (mm)	Top thickness (mm)	Wall thickness (mm)	Infill (%)	Infill Pattern	Material volume (%)
Creality Ender 3	PLA	Tucab PLA Green	3	25	5	0.4	0.2	0.4	0.4	0.8	0	None	31.85
			3	25	5	0.4	0.2	0.4	0.4	0.8	10	Cubic	38.66
			3	25	5	0.4	0.2	0.4	0.4	0.8	20	Cubic	45.48
			3	25	5	0.4	0.2	0.4	0.4	0.8	35	Cubic	55.70
			3	25	5	0.4	0.2	0.4	0.4	0.8	50	Cubic	65.92
			3	25	5	0.4	0.2	0.4	0.4	0.8	100	None	100.00
			3	25	5	0.4	0.2	0.2	0.2	0.4	0	None	16.42
			3	25	5	0.4	0.2	0.2	0.2	0.4	10	Cubic	24.78
			3	25	5	0.4	0.2	0.2	0.2	0.4	20	Cubic	33.14
			3	25	5	0.4	0.2	0.4	0.4	0.8	30	Cubic	52.29
	PETG	Tucab PETG Black	3	25	5	0.4	0.2	0.4	0.4	0.8	0	None	31.85
			3	25	5	0.4	0.2	0.4	0.4	0.8	10	Cubic	38.66
			3	25	5	0.4	0.2	0.4	0.4	0.8	20	Cubic	45.48
			3	25	5	0.4	0.2	0.4	0.4	0.8	35	Cubic	55.70
			3	25	5	0.4	0.2	0.4	0.4	0.8	50	Cubic	65.92
			3	25	5	0.4	0.2	0.4	0.4	0.8	100	None	100.00
Ultimaker 3 Extended	PLA	Filamentive PLA Grey	3	25	5	0.4	0.2	0.4	0.4	0.8	0	None	31.85
			3	25	5	0.4	0.2	0.4	0.4	0.8	10	Cubic	38.66
			3	25	5	0.4	0.2	0.4	0.4	0.8	20	Cubic	45.48
			3	25	5	0.4	0.2	0.4	0.4	0.8	35	Cubic	55.70
			3	25	5	0.4	0.2	0.4	0.4	0.8	50	Cubic	65.92
			3	25	5	0.4	0.2	0.4	0.4	0.8	100	None	100.00
			3	25	5	0.4	0.2	0.2	0.4	0.4	0	None	22.85
			3	25	5	0.4	0.2	0.2	0.4	0.4	10	Cubic	30.56
			3	25	5	0.4	0.2	0.2	0.4	0.4	20	Cubic	38.28
			3	25	5	0.4	0.2	0.2	0.4	0.4	30	Cubic	45.99
	PETG	3D Filkemp PETG Transparent	3	25	5	0.4	0.2	0.4	0.4	0.8	0	None	31.85
			3	25	5	0.4	0.2	0.4	0.4	0.8	10	Cubic	38.66
			3	25	5	0.4	0.2	0.4	0.4	0.8	20	Cubic	45.48
			3	25	5	0.4	0.2	0.4	0.4	0.8	35	Cubic	55.70
			3	25	5	0.4	0.2	0.4	0.4	0.8	50	Cubic	65.92
			3	25	5	0.4	0.2	0.4	0.4	0.8	100	None	100.00
	Nylon	Ultimaker Nylon Black	3	25	5	0.4	0.2	0.3	0.3	0.8	0	Cubic	25.65
			3	25	5	0.4	0.2	0.3	0.3	0.8	10	Cubic	33.09
			3	25	5	0.4	0.2	0.3	0.3	0.8	20	Cubic	40.52
			3	25	5	0.4	0.2	0.3	0.3	0.8	35	Cubic	51.67
			3	25	5	0.4	0.2	0.3	0.3	0.8	50	Cubic	62.82
			3	25	5	0.4	0.2	0.3	0.3	0.8	100	None	100.00